Electronic Supplementary Information

S 1. Experimental details

S 1.1 General information

All products and solvents were purchased from standard sources and directly used without further purification. ^{1}H- and ^{13}C-NMR spectra were recorded on a Bruker AvanceIII 500 MHz instrument and peaks were referenced to residual solvent peaks. High resolution mass spectra were measured in the positive mode on an FTMS Bio APEX II from Bruker with electrospray ionization (HR-ESI). Elemental analysis was performed with a FLASH 2000 organic elemental analyser from Thermo Scientific. X-ray diffraction data were measured on a SuperNova, Dual, Cu at home/near, Atlas diffractometer. The crystal was kept at a steady T = 140.01(10) K during data collection. The structure was solved with the **ShelXT**[1] solution program using dual methods and by using **Olex2** 1.5[2] as the graphical interface. The model was refined with **ShelXL** 2018/3[3] using full matrix least squares minimisation on F^2. UV-Vis spectra were recorded on a Perkin Elmer Lambda 40 spectrometer. Cyclic voltammetry experiments were performed using an Autolab PGSTAT- 100N potentiostat and controlled potential electrolysis experiments were recorded on a BioLogic SP300 potentiostat. The amount of H_2 produced during bulk electrolysis experiments was analysed with a Perkin-Elmer Clarus 500 gas chromatographer (GC). The amount of hydrogen evolved during the photocatalysis was determined by gas chromatography with a Perkin Elmer GC Clarus 580, using a column molecular sieve 5 Å of 30 m x 0.53 mm, an oven operating isothermally at 30 °C and a TCD detector operating at 150°C with Ar carrier. The results were validated with at least two sets of independent measurements.

S 1.2 Electrochemistry

Cyclic voltammograms were recorded in CH_3CN in the presence 0.1 M $TBAPF_6$ as supporting electrolyte under inert atmosphere (N_2). A setup with three electrodes consisting of glassy carbon as working electrode, platinum wire as counter electrode and an Ag/AgCl (KCl 3 M) reference electrode was used. Ferrocene was used as internal standard. Controlled potential coulometry was carried out in a two-compartment cell, with the mercury pool working electrode separated by a porous frit from the coiled platinum wire counter electrode. In the working compartment, 8 mL of CH_3CN containing 0.1 M of $TBAPF_6$, 1 mM of catalyst and 100 mM of TFA were used for the measurements. The solution was degassed with N_2 for 30 minutes and during the experiment the cell was continuously purged with N_2 (5 mL min^{-1}). The headspace was analyzed every two minutes with the GC for 4 hours.

S 1.3 Photocatalysis

The experiments were carried out in a water jacketed flask containing 6 mL solution of 1 M acetate buffer (pH = 4), 0.5 mM $[Ru(bpy)_3]Cl_2$, 0.1 M ascorbic acid and 5 μM catalyst. The solution was purged with Ar for 40 minutes prior to the experiment and the samples were irradiated with a 1.1 W LED light (475 nm) under constant stirring. A chilling circulator unit was used to keep the reaction in the jacketed vessel at constant temperature (20°C). The headspace was analyzed by periodically sampling 50 μL with a Hamilton sample lock syringe along 6 h.

S 2. Syntheses

S 2.1 Synthesis of the Ligands

N,N-Bis-(6-(2,2'-bipyridyl)methyl)amine[4] and 2-Acetoxy-(6-bromomethyl)pyridine[5] were synthesized according to reported procedures.

Ligand L2.

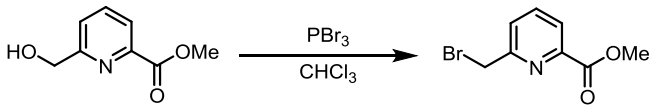

a) To a solution of Methyl-6-hydroxymethyl-2-carboxylate pyridine (400 mg, 2.4 mmol) in anhydrous CH_2Cl_2 (50 mL) was added PBr_3 (0.680 mL, 7.2mmol) at 0°C. The reaction mixture was stirred for 12 h at room temperature. The solvent was removed by rotary evaporation, and the resulting residue suspended in water and then neutralized with an aqueous saturated Na_2CO_3 solution. After extraction with CH_2Cl_2 (3 x 100 mL), the combined organic layers were dried with Na_2SO_4 and the solvent was removed under reduced pressure, leading to Methyl-6-(bromomethyl)-2-pyridinecarboxylate as white solid (386 mg, 70%) used without further purification.[6]

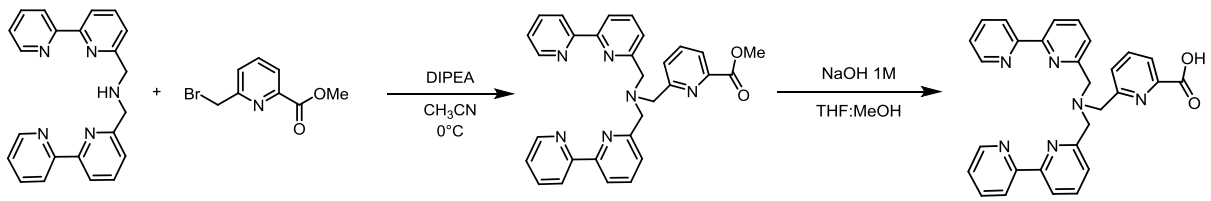

b) Methyl 6-(bromomethyl)-2-pyridinecarboxylate (368 mg, 1.7 mmol) was added to a solution of *N,N*-Bis-(6-(2,2'-bipyridyl)methyl)amine[4] (498 mg, 1.41 mmol) in CH_3CN (50 mL) at room temperature. The base *N,N*-diisopropylethylamine (0.591 mL, 3.4 mmol) was added dropwise at 0°C and the mixture was stirred at room temperature overnight. The solvent was removed and the crude was suspended in water (20 mL) and extracted with ethyl acetate (3 x 50 mL), the organic phases were then washed with brine and dried over anhydrous Na_2SO_4, filtered and concentrated. The crude

compound was purified by filtration over alumina (CH_2Cl_2, EtOAc 0-100%) to give 403 mg (57% yield). The ester obtained was hydrolyzed with NaOH (160 mg, 4 mmol) in THF/MeOH/H_2O (15 mL, 15 mL, 45mL) at 50°C for 4 h. The reaction mixture was acidified at pH 2 using HCl and **L2** was obtained pure as a white precipitate (367 mg, 94% yield).

^{1}H NMR (CD_3OD, 500 MHz): δ (ppm) 8.69 (m, 2H), 8.13 (d, J= 8.02 Hz, 2H), 7.95 (m, 3H), 7.89 (m, 2H), 7.85 (m, 4H), 7.8 (m, 3H), 7.42 (m, 1H), 7.37 (m, 4H), 3.98 (s, 2H), 3.95 (s, 4H).

^{13}C NMR (CD_3OD, 125 MHz): δ (ppm) 172.60, 160.09, 158.79, 156.75, 156.58, 156.12, 151.56, 139.21, 138.88, 138.80, 125.20, 125.14, 124.74, 123.55, 122.70, 121.09, 60.84.

HRESI-MS (m/z) : 489.2031 ([M-H]$^+$, calcd for $[C_{29}H_{25}N_6O_2]^+$: 489.2039).

a) ^{13}C-NMR

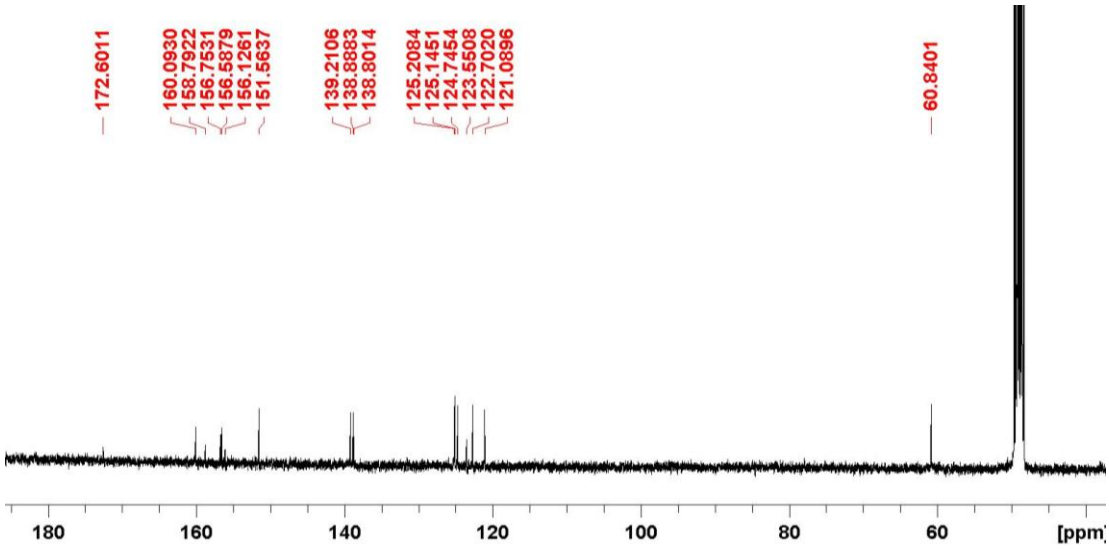

b) ^{1}H-NMR

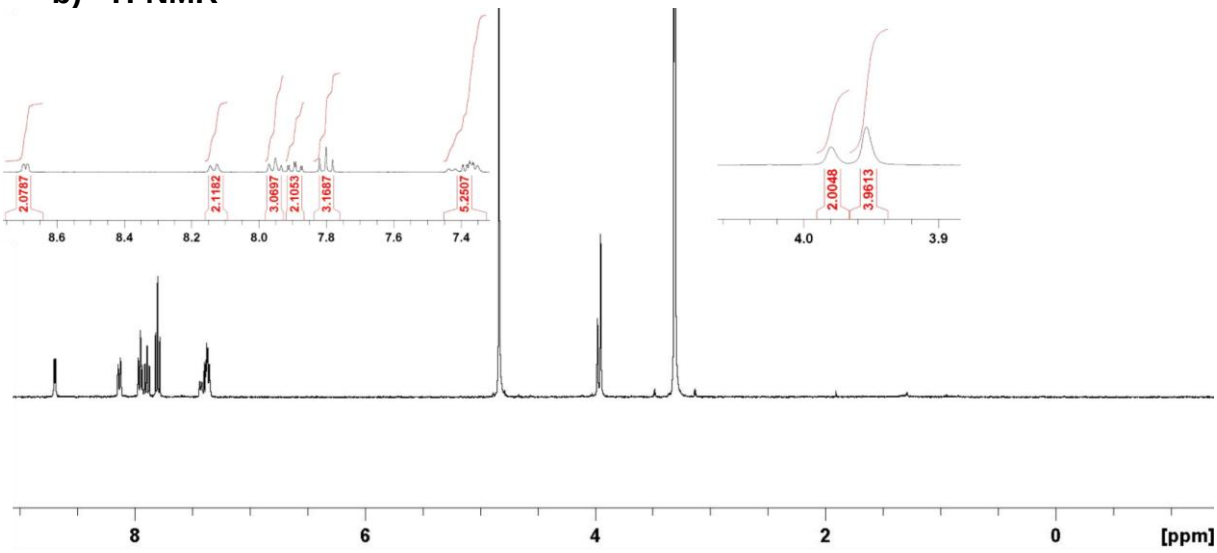

Ligand L3.

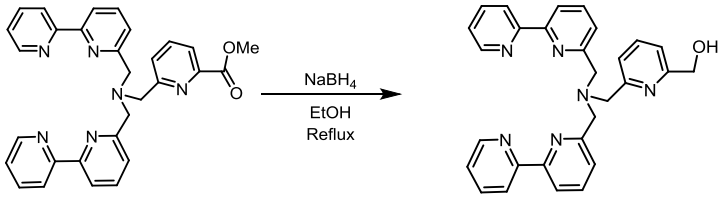

Ligand **L3** was synthesized through reduction of the ester precursor of **L2**. The ester (250 mg, 0.5 mmol) was dissolved in ethanol and $NaBH_4$ was added slowly. The mixture was stirred at 78°C overnight. Then the solvent was removed and CH_2Cl_2 (20 mL) and water (10 mL) were added. The compound was extracted in the organic phase washed with brine and dried over Na_2SO_4. After filtration and evaporation, the crude was purified by column chromatography (Al_2O_3, CH_2Cl_2 : EtOAc 70:30). The product was obtained as white solid (187 mg, 79% yield).

^{1}H NMR (CD_3CN, 500 MHz): δ (ppm) 8.59 (m, 2H), 8.38 (m, 2H), 8.21 (m, 2H), 7.79 (m, 4H), 7.68 (t, J = 7.69 Hz, 1H), 7.59 (m, 2H), 7.53 (d, H = 7.57 Hz, 1H), 7.31 (m, 2H), 7.21 (d, J = 7.69 Hz, 1H), 4.59 (s, 2H), 3.94 (s, 4H), 3.92 (s, 2H).

^{13}C NMR (CD_3CN, 125 MHz): δ (ppm) 160.27, 159.36, 158.93, 156.36, 155.50, 149.55, 137.77, 137.47, 137.34, 124.19, 123.60, 121.61, 121.05, 119.26, 118.90, 64.56, 60.28, 60.25.

HRESI-MS (m/z): 475.2250 ($[M-H]^+$, calcd for $[C_{29}H_{27}N_6O]^+$: 475.2246).

a) ^{13}C-NMR

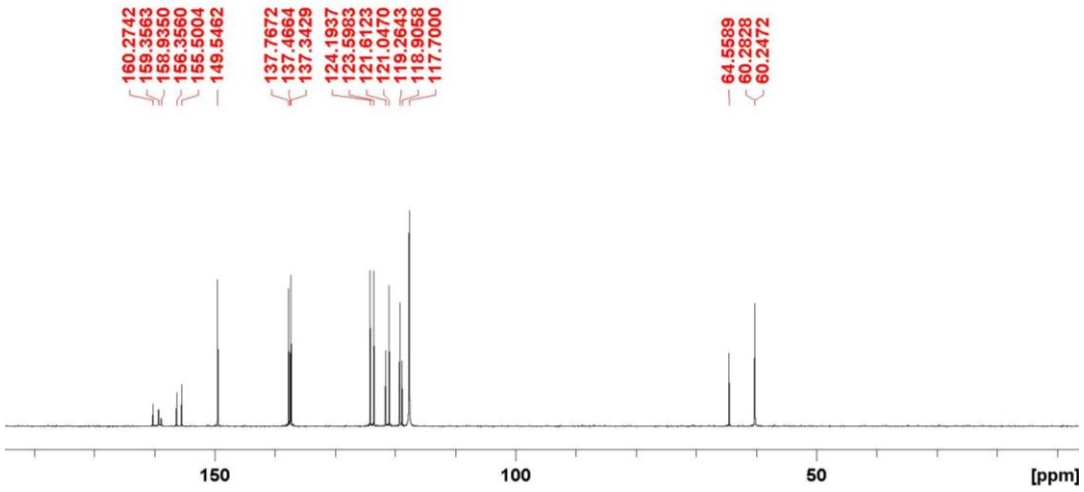

b) ^{1}H-NMR

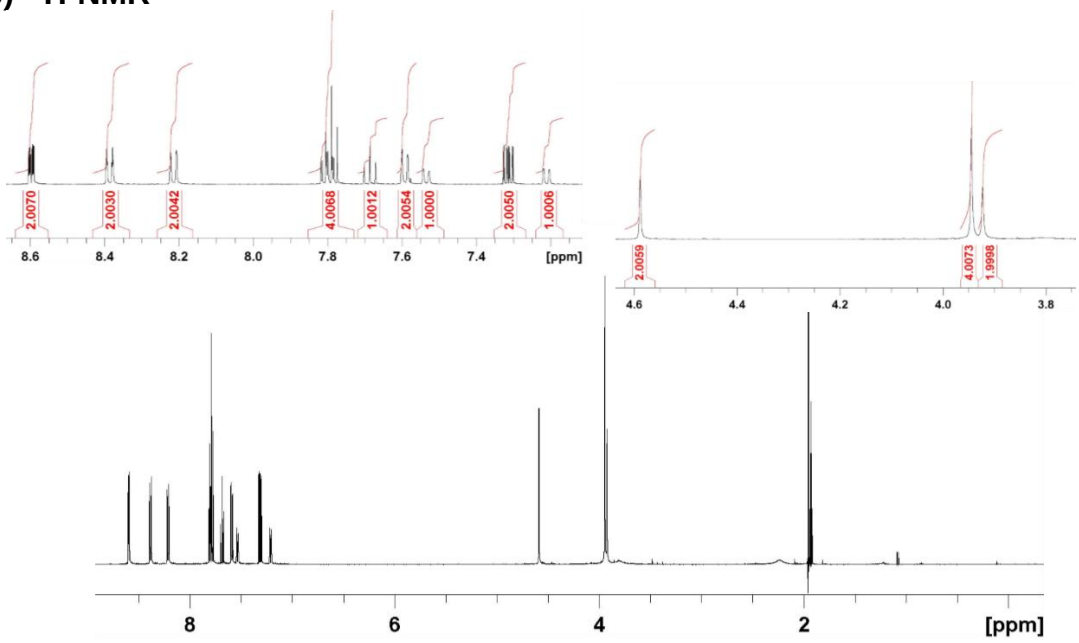

Ligand L4.

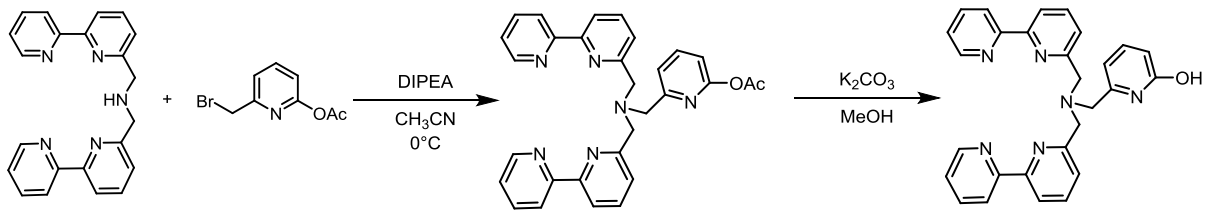

2-Acetoxy-(6-bromomethyl)pyridine[5] (179 mg, 0.72 mmol) and of *N,N*-Bis-(6-(2,2'-bipyridyl)methyl)amine[4] (204 mg , 0.56 mmol) were mixed together in CH_3CN (50 mL) at room temperature and *N,N*-diisopropylethylamine (0.234 mL, 1,35 mmol) was added dropwise at 0°C. The reaction mixture was stirred at room temperature for 15 h. The solvent was removed by rotary evaporation and the resulting residue was dissolved in water. The product was extracted into ethyl acetate (3 x 50 mL) and washed with brine (2 x 30 mL). The combined organic phases were dried over anhydrous Na_2SO_4, filtered and evaporated under reduced pressure to afford the crude compound used in the next reaction without further purification. The compound (238 mg, 0.48 mmol) was dissolved in MeOH, K_2CO_3 (238 mg, 2.4 mmol) was added and the reaction was stirred for 4h. The solvent was evaporated and the crude was dissolved in water and extracted three times with EtOAc (20 mL). The combined organic layers were dried over Na_2SO_4 and concentrated. The product was purified by column chromatography on alumina ($CHCl_3$: MeOH, 98:2) to give 188 mg (85% yield) of **L4**.

^{1}H NMR (CD_2Cl_2, 500 MHz): δ (ppm) 8.65 (m, 2H), 8.61 (m, 2H), 8.33 (d, J= 7.53 Hz, 2H), 7.86 (m, 2H), 7.82 (t, J = 7.86, 2H), 7.42 (d, J = 7.76 Hz, 2H), 7.30 (m, 3H), 6.32 (d, J = 9.12 Hz, 1H), 6.02 (d, J = 6.68 Hz, 1H), 3.98 (s, 4H), 3.75 (s, 2H).

^{13}C NMR (CD_2Cl_2, 125 MHz): δ (ppm) 163.07, 157.49, 155.90, 155.87, 149.14, 145.26, 140.63, 137.57, 137.06, 123.84, 123.60, 121.31, 119.65, 119.22, 104.11, 59.28, 53.97.

HRESI-MS (m/z): 461.2087 ([M-H]$^+$, calcd for $[C_{28}H_{25}N_6O]^+$: 461.2090).

a) ^{13}C-NMR

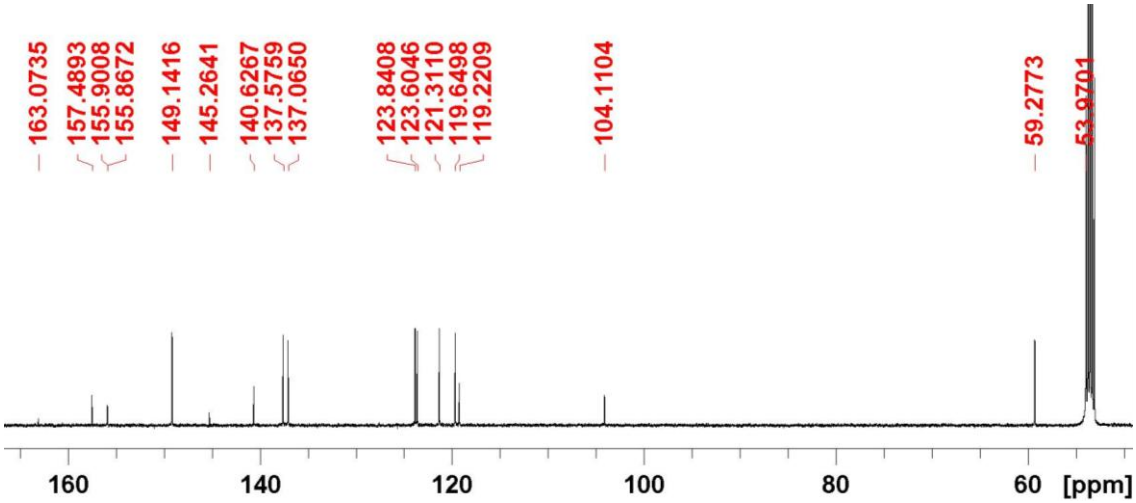

b) ^{1}H-NMR

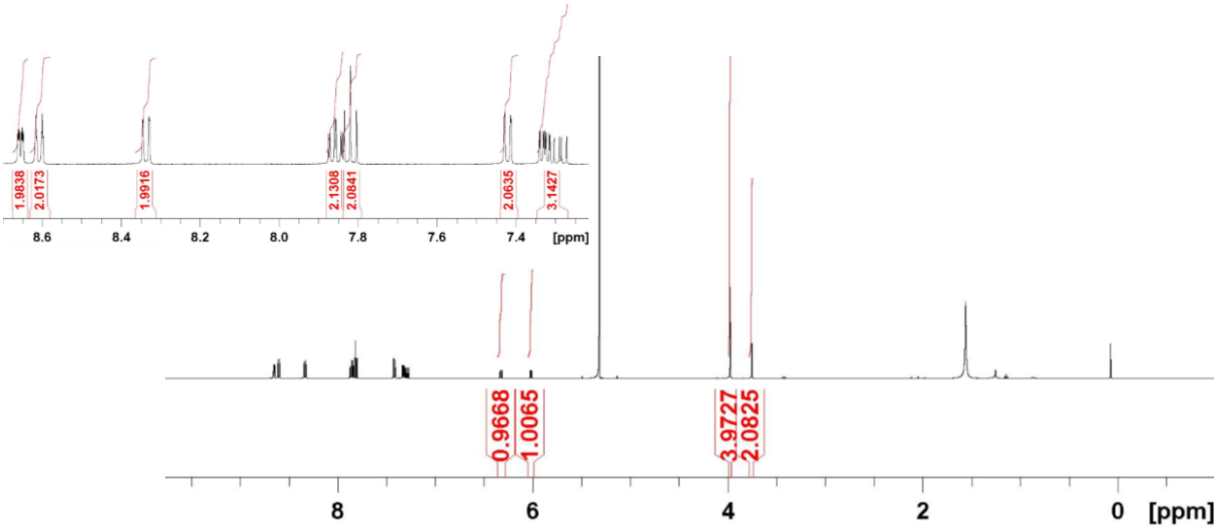

S 2.2 Synthesis of the complexes

A general procedure was used to synthesize the complexes. To a solution of the ligand dissolved in MeOH were added 1.2 equivalents of $CoSO_4 \cdot 7H_2O$ or $Co(BF_4)_2 \cdot 6H_2O$ and the mixture was stirred overnight. The product was precipitated after the addition of diethyl ether, the filtrate was washed with diethyl ether and dried under reduced pressure.

***C2*. L2** (300mg, 0.6 mmol) and $Co(BF_4)_2 \cdot 6H_2O$ (224 mg, 0.66 mmol) gave 307 mg (81 % yield) as slightly pink powder.

HRESI-MS (m/z) : 546.1216 ($[M]^+$, calcd for $[C_{29}H_{23}CoN_6O_2]^+$: 546.1214).

Elemental Analysis: calcd (%) for $[C_{29}H_{23}BCoF_4N_6O_2]$: C 55.00, H 3.66, N 13.27; found C 55.32, H 3.75, N 13.22.

***C3*. L3** (150 mg, 0.3 mmol) and $Co(BF_4)_2 \cdot 6H_2O$ (118 mg, 0.35 mmol) gave 176 mg (83 % yield) as pink solid.

HRESI-MS (m/z) : 620.1527 ($[M\text{-}BF_4]^+$, calcd for $[C_{29}H_{26}BCoF_4N_6O]^+$: 620.1529).

Elemental Analysis**:** calcd (%) for $[C_{29}H_{26}B_2CoF_8N_6O]$: C 49.26, H 3.71, N 11.89; found C 49.39, H 3.81 N 11.48.

***C3'*. L3** (150 mg, 0.3 mmol) and $CoSO_4 \cdot 7H_2O$ (49 mg, 0.32 mmol) gave 149 mg (79 % yield).

HRESI-MS (m/z) : 266-5751 ($[M\text{-}SO_4]^{2+}$, calcd for $[C_{29}H_{26}CoN_6O]^{2+}$: 266.5750).

Elemental Analysis**:** calcd (%) for [$C_{29}H_{26}CoN_6O_5S$]: C 55.33, H 4.16, N 13.35; found C 55.76, H 4.37 N 13.16.

***C3''*. C3'** (100 mg, 0.16 mmol) was dissolved in 2 mL of water and NH_4PF_6 (239 mg, 0.64 mmol) was added to the solution. The precipitate was filtered and washed with diethyl ether to afford 176 mg of pure **C3"** (77% yield).

HRESI-MS (m/z) : 678.1140 ([M-PF_6]$^+$, calcd for [$C_{29}H_{26}CoF_6N_6OP$]$^+$: 678.1142).

Elemental Analysis**:** calcd (%) for [$C_{29}H_{26}CoF_{12}N_6OP_2$]: C 42.30, H 3.18, N 10.21; found C 42.08, H 3.39 N 10.29.

***C4*. L4** (90 mg, 0.2 mmol) and $Co(BF_4)_2 \cdot 6H_2O$ (73 mg, 0.21 mmol) gave 127 mg (92 % yield) as pink solid.

HRESI-MS (m/z) : 606.1376 ([M-H]$^+$, calcd for [$C_{28}H_{24}BCoF_4N_6O_2$]$^+$: 606.1373).

Elemental Analysis**:** calcd (%) for [$C_{28}H_{24}B_2CoF_8N_6O$]: C 48.52.14, H 3.49, N 12.13; found C 48.25, H 12.07, N 12.51.

***C4'*. L4** (90 mg, 0.2 mmol) and $CoSO_4 \cdot 7H_2O$ (32 mg, 0.21 mmol) gave 119 mg (84 % yield) as pink solid

HRESI-MS (m/z) : 259.5670 ([M-H]$^{2+}$, calcd for [$C_{28}H_{24}CoN_6O$]$^{2+}$ 259.5672).

Elemental Analysis**:** calcd (%) for [$C_{30}H_{36}CoN_6O_9S$]: C 50.35, H 5.07, N 11.74; found C 49.85, H 4.91, N 12.03 (2MeOH and 2H_2O).

S 3. Evans method

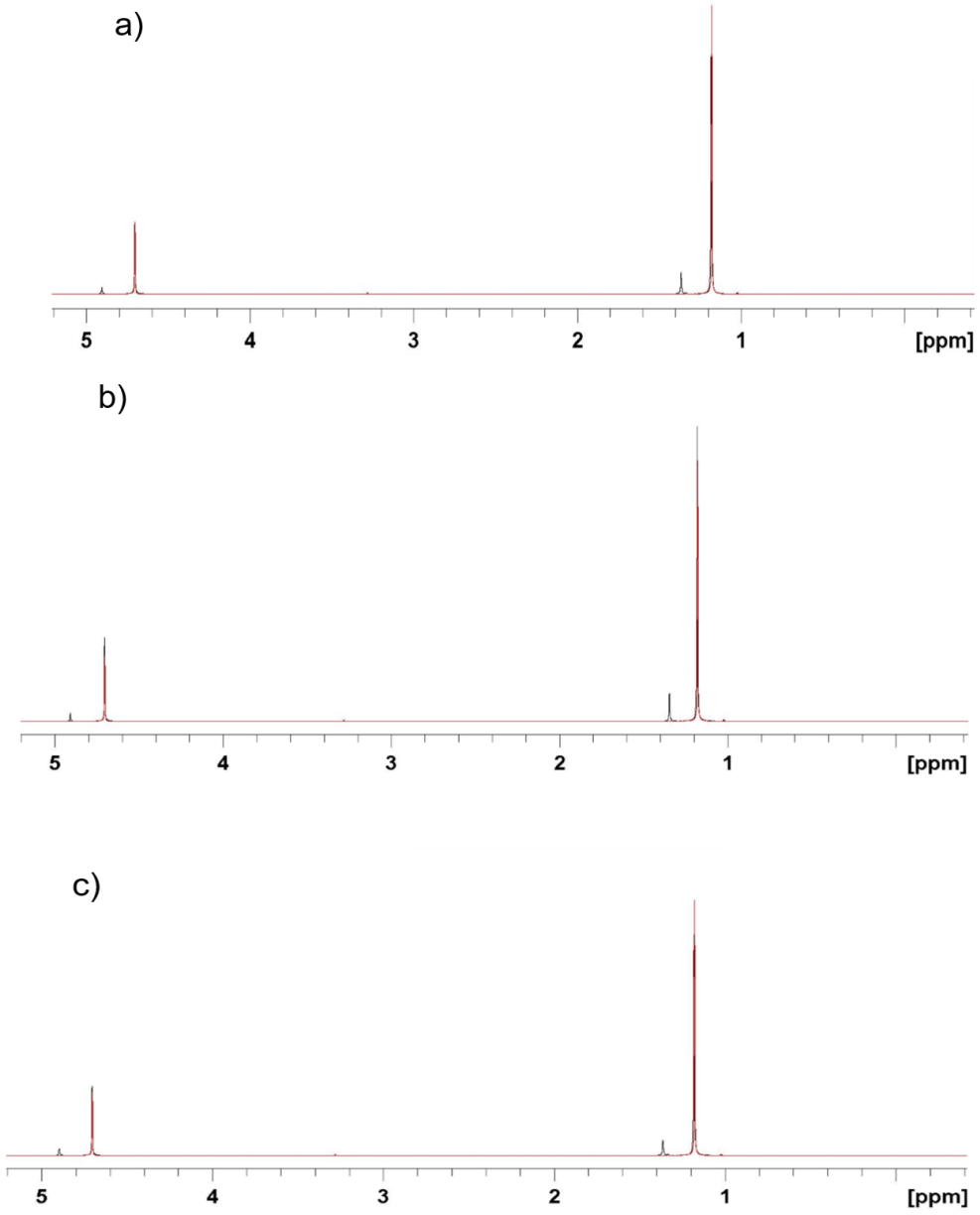

Figure ES1. Determination of the magnetic moment with the Evans Method using a previously described calculation.[7-10] Red: tube containing a solution of *t*-butanol and D_2O (30 μL of *t*-butanol and

970 μL of D_2O). Black: tube containing a solution of *t*-butanol and D_2O (30 μL of *t*-butanol and 970 μL of D_2O) with a coaxial insert containing a solution of *t*-butanol and the complex (**C2** a), **C3** b), **C4** c)) in D_2O (4.2 mg of complex and 30 μL of *t*-butanol and adjust total volume to 1 mL with D_2O).

S 4. Electrochemistry

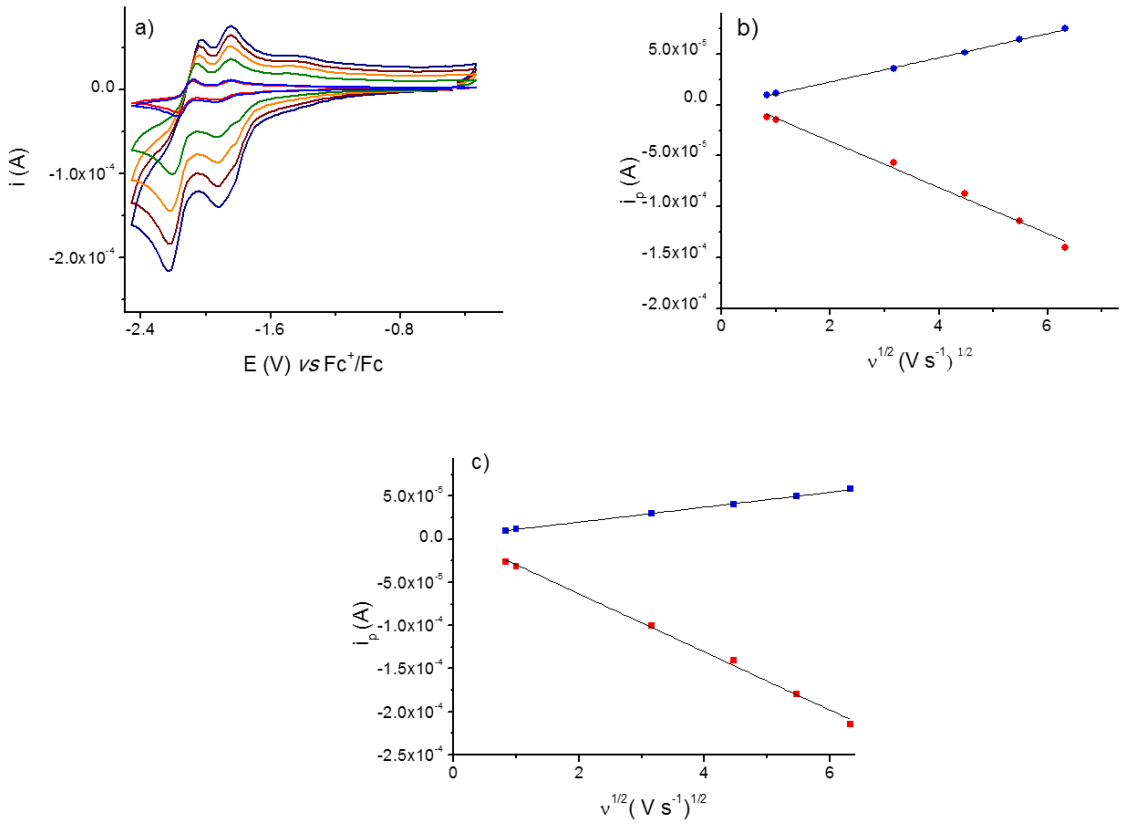

Figure ES2. a) CV of 1 mM **C2** in acetonitrile, 0.1 M $TBAPF_6$ at 0.7 (—), 1 (—), 10 (—), 20 (—), 30(—) and 40(—) V s^{-1} and glassy carbon as working electrode. Cathodic (red) and anodic (blue) peak currents (i_{pa} and i_{pc}) for the first (b) and second (c) wave versus the square root of scan rate ($\nu^{1/2}$).

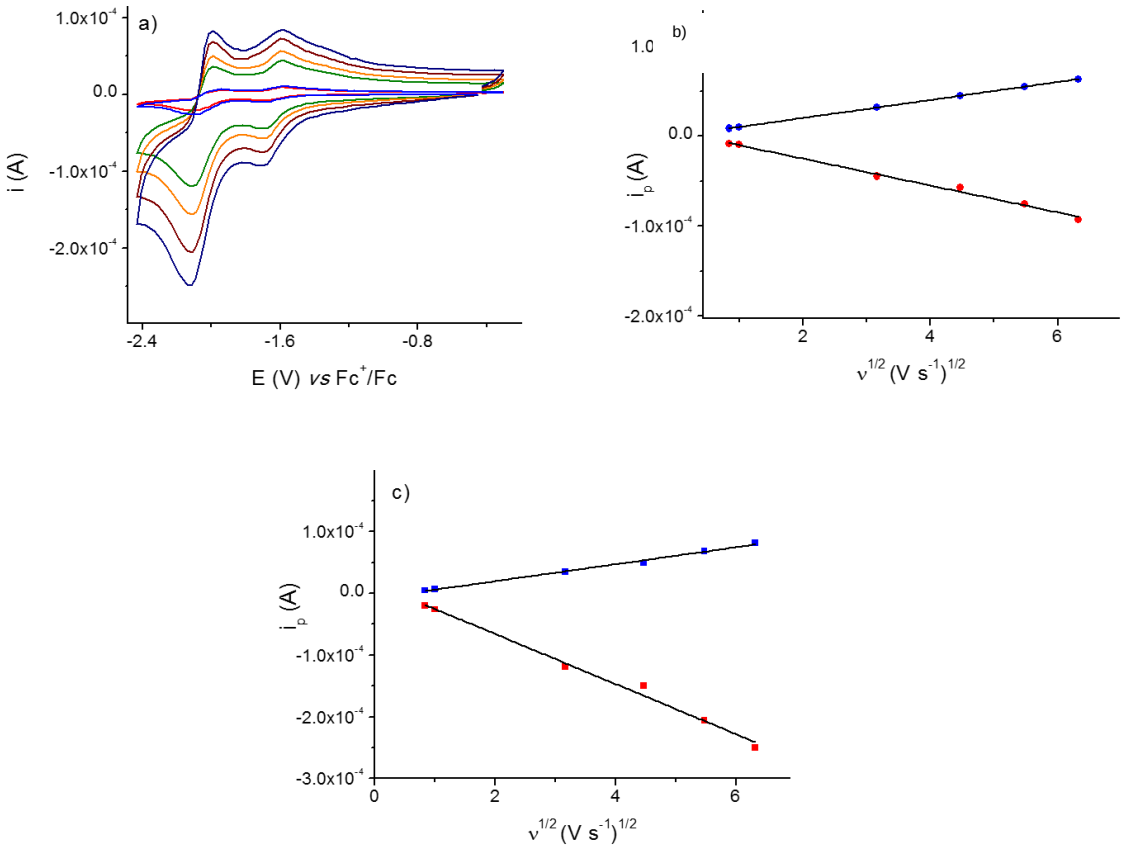

Figure ES3. a) CV of 1 mM **C3** in ACN 0.1 M $TBAPF_6$ at 0.7 (—), 1 (—), 10 (—), 20 (—), 30(—) and 40(—) V s^{-1} and glassy carbon as working electrode. Cathodic (red) and anodic (blue) peak currents (i_{pa} and i_{pc}) for the first (b) and second (c) wave versus $\nu^{1/2}$.

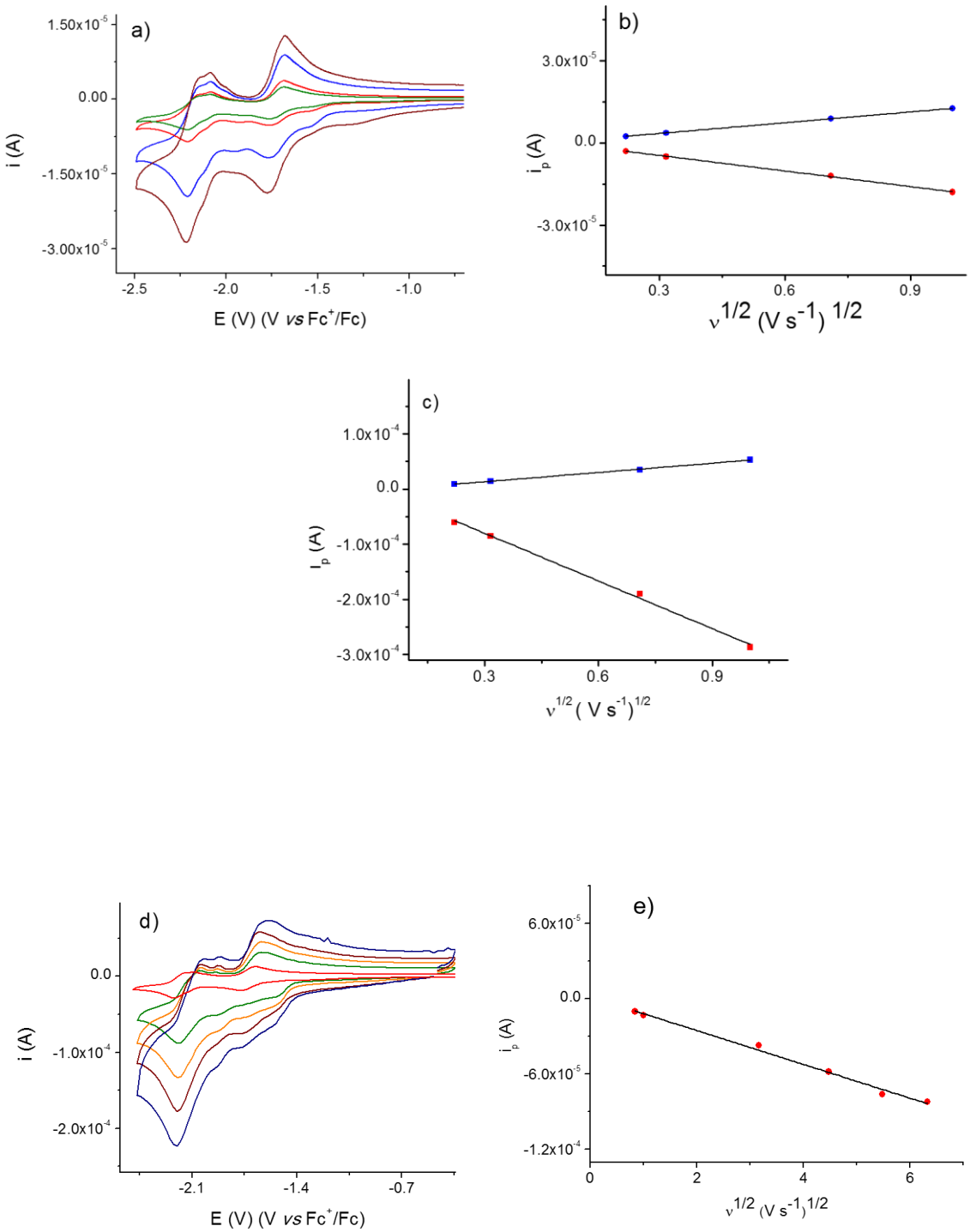

Figure ES4. a) CV of 1 mM **C4** in ACN 0.1 M $TBAPF_6$ at 0.05 (—), 0.1 (—), 0.5 (—) and 1 (—)V s^{-1}, d) CV of 1 mM **C4** in ACN 0.1 M $TBAPF_6$ at 0.7 (—), 1 (—), 10 (—), 20 (—), 30(—) and 40(—) V s^{-1} and glassy carbon as working electrode; b) and e) show the cathodic (red) and anodic (blue) peak currents (i_{pa} and i_{pc}) for the first wave versus $\nu^{1/2}$; c) displays i_{pa} and i_{pc} for the second wave versus $\nu^{1/2}$.

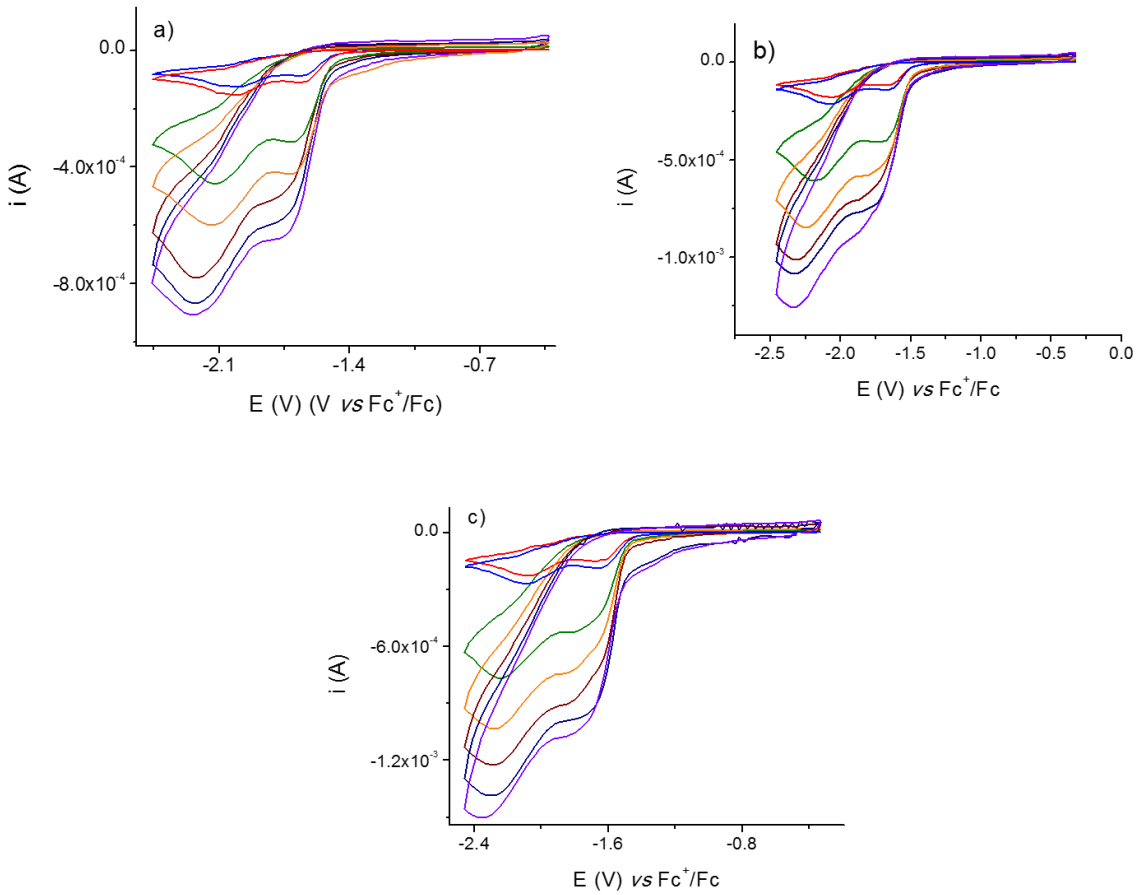

Figure ES5. CVs of **C2** (1 mM) in ACN at 10 (a), 15 (b), and 20 (c) mM of TFA and at 0.7 (—), 1 (—), 10 (—), 20 (—), 30(—), 40(—) and 47 (—) V s^{-1}. The experiments were performed under Ar in the presence of 0.1 M $TBAPF_6$ as supporting electrolyte and glassy carbon as working electrode.

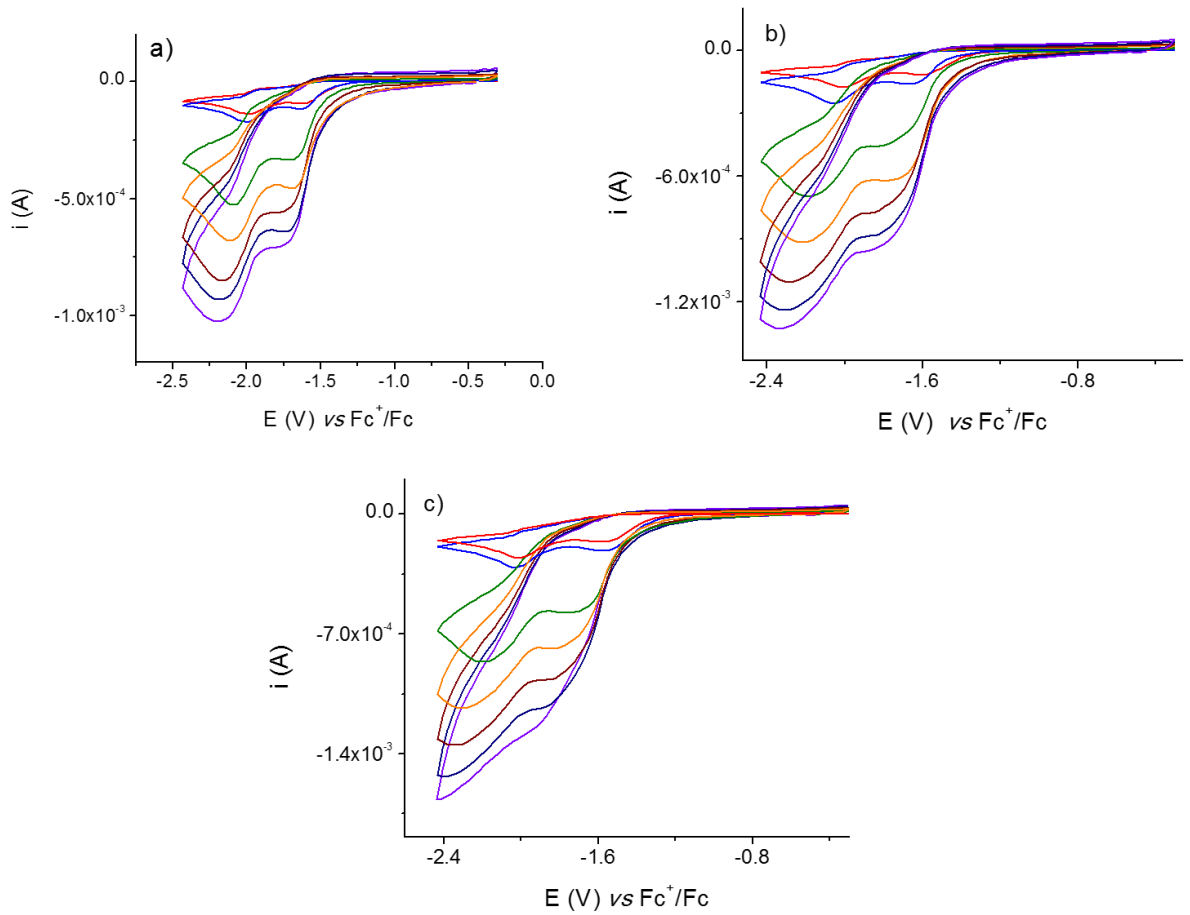

Figure ES6. CVs of **C3** (1 mM) in ACN at 10 (a), 15 (b), and 20 (c) mM of TFA and at 0.7 (—), 1 (—), 10 (—), 20 (—), 30(—), 40(—) and 47 (—) V s^{-1}. The experiments were performed under Ar in the presence of 0.1 M $TBAPF_6$ as supporting electrolyte and glassy carbon as working electrode.

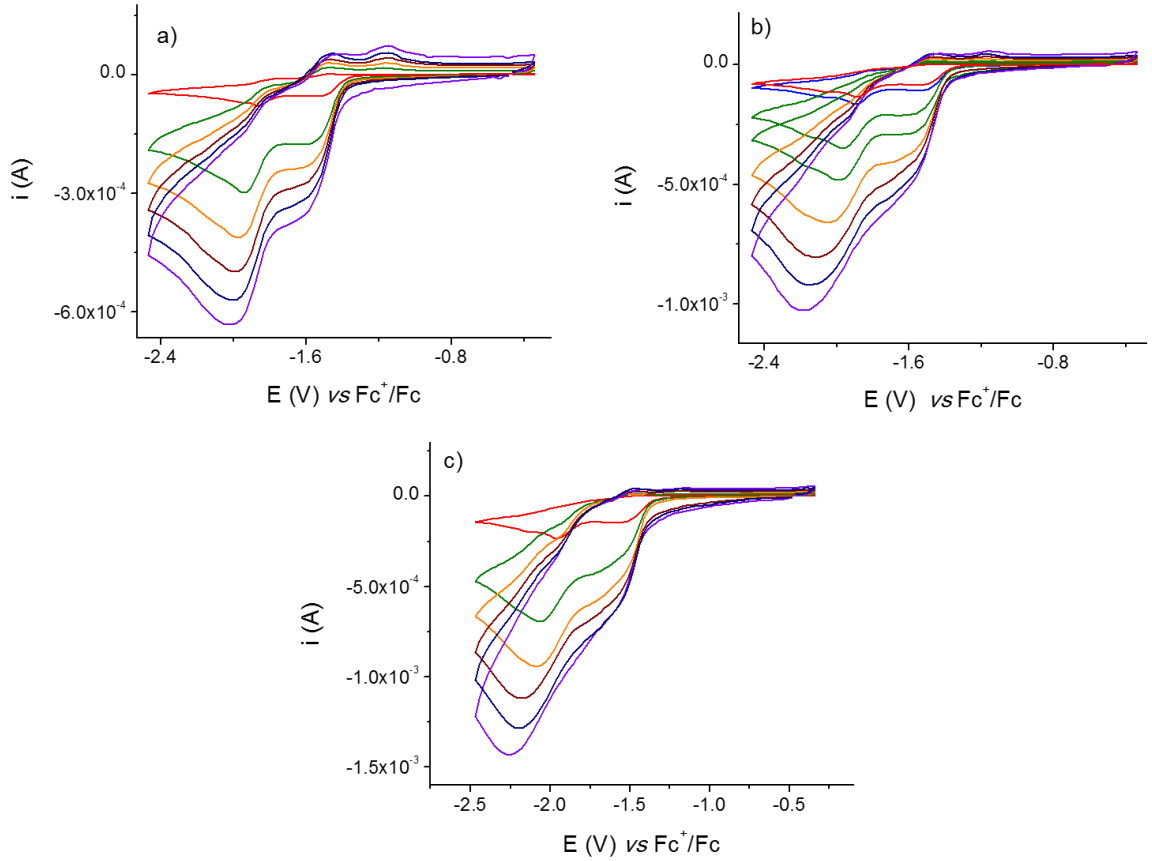

Figure ES7. CVs of **C4** (1 mM) in ACN at 5 (a), 10 (b), and 15 (c) mM of TFA and at 1 (—),10 (—), 20 (—), 30(—), 40(—) and 47 (—) V s^{-1}. The experiments were performed under Ar in the presence of 0.1 M $TBAPF_6$ as supporting electrolyte and glassy carbon as working electrode.

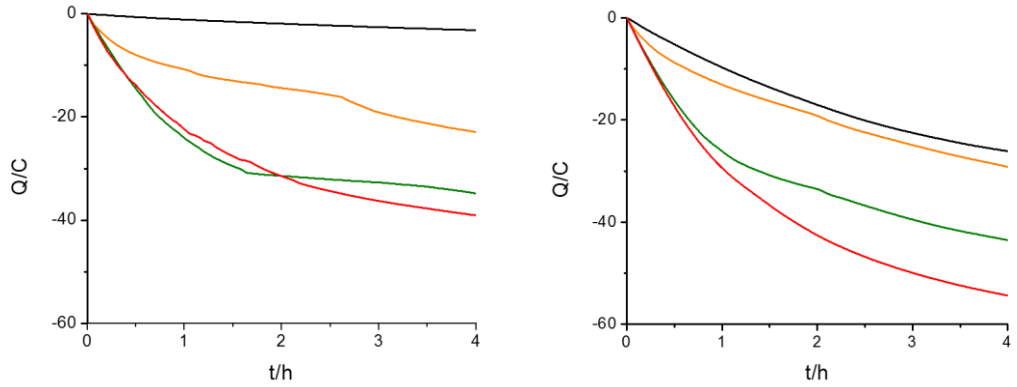

Figure ES8. Charge versus time for bulk electrolysis at -1.5 (left) and -1.63 (right) V vs Fc^+/Fc for **C2** (—), **C3** (—) and **C4** (—), and blank (— no catalyst only 100 mM of TFA). The experiments were performed in 8 mL solutions in the presence of 1 mM complex in CH_3CN with 0.1 M $TBAPF_6$ and 100 mM TFA using a pool of mercury as working electrode, Ag/AgCl (3M NaCl) as reference electrode and a platinum wire as counter electrode separated by a porous glass frit.

Table ES1. Faradaic yield and TON reached during bulk electrolysis experiments at -1.5 and -1.63 V vs Fc^+/Fc after 4 h.

Cat.	$E_{(electr.)}$	Faradaic yield	TON
C2	-1.5	51%	16
	-1.63	92%	19
C3	-1.5	73%	25
	-1.63	85%	24
C4	-1.5	53%	19
	-1.63	85%	30

S 5. Foot-of-the-wave analysis

The catalytic wave recorded for **C3** can give information about the kinetics of the hydrogen evolution assuming a multi-step reaction where all the electron transfers occur at the electrode. As the potentials at half of the catalytic waves (E_{cat}) are found at more positive values than $Co^{II/I}$, the most likely mechanism appears to be an ECEC mechanism with the second reduction being easier than first one. According to this mechanistic scenario, foot-of-the wave analysis (FOWA) can be utilized to determine the rate constant of the first protonation (k_1).[11-14] In the plot of (i_{cat}/i_p) versus 1/ {1 + exp [F/RT(E - E_{cat})]}, (where i_p is the peak current of a non-catalytic wave in the absence of acid and i_{cat} is the catalytic current) the part near the foot of the catalytic wave can be linearly fitted. The slope of this linear fit allows for the determination of the rate constant (k_1) according to equations (Eq. 5.1) and (Eq. 5.2). The rate constant k_1 for catalyst **C3** was calculated in the presence of various concentrations of acid and at different scan rates. Figure ES9 clearly displayed that the rate constants obtained are independent of the scan rate and the acid concentration, thus ensuring the reliability of the values. The rate constant for the second protonation step (k_2) was then estimated from the potential shift between the catalytic wave (E_{cat}) and the triggering redox wave ($E_{CoII/I}$), according to equation 5.3. The reliability of the present procedure was finally confirmed by comparing the k_2

value extracted using equation 5.4 from the plateau current of the cyclic voltammetry of **C3** with 20 mM TFA estimated under scan rate independent conditions (Figure ES11b).

For complexes **C2** and **C4**, because of the consistent shift of the catalytic wave with respect to the Co(II)/Co(I) reduction, estimation of k_2 was made using eq 5.4 from the plateau current extrapolated under scan rate independent conditions (Figure ES11a,c).

$$\frac{i_{cat}}{i_p} = \frac{4{,}48\sqrt{\frac{k_1 RT}{F\,v}}}{1+\exp[\frac{F}{RT}(E-E_{cat})]} \qquad \text{(Eq. 5.1)}$$

$$slope = 4{,}48\sqrt{\frac{k_1 RT}{F\,v}} \qquad \text{(Eq. 5.2)}$$

$$E_{cat} = E_{CoII/I} + \frac{RT}{F}\,ln\left(1+\sqrt{\frac{k_1}{k_2}}\right) \qquad \text{(Eq. 5.3)}$$

$$i_{pl} = 2FSC_{cat}\sqrt{D_{cat}}\sqrt{k_2 C_A^0} \qquad \text{(Eq. 5.4)}$$

F : Faraday Constant;
R: Gas constant;
T: temperature;
C_A^0 : concentration of acid;
k_1,k_2 : observed rate constants.
ν : scan rate;
E : electrode potential;
E_{cat} : half-wave potential of the catalytic wave;
$E_{CoII/I}$: potential of the first reduction of the catalyst;
i_{cat} : catalytic current;
i_p : peak current of a non-catalytic wave.
i_{pl} = plateau current
D_{cat} = diffusion coefficient of the catalyst

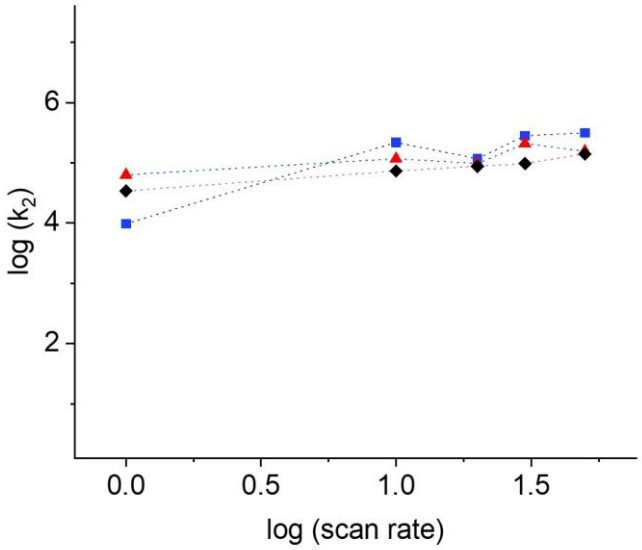

Figure ES9. k_2 values obtained through FOWA for **C3** at 0.7, 5, 10, 20, 30, 50 V s^{-1} in the presence of 10 (blue) 15 (red) 20 (black) mM of TFA under the conditions shown in the CVs in **ES6**.

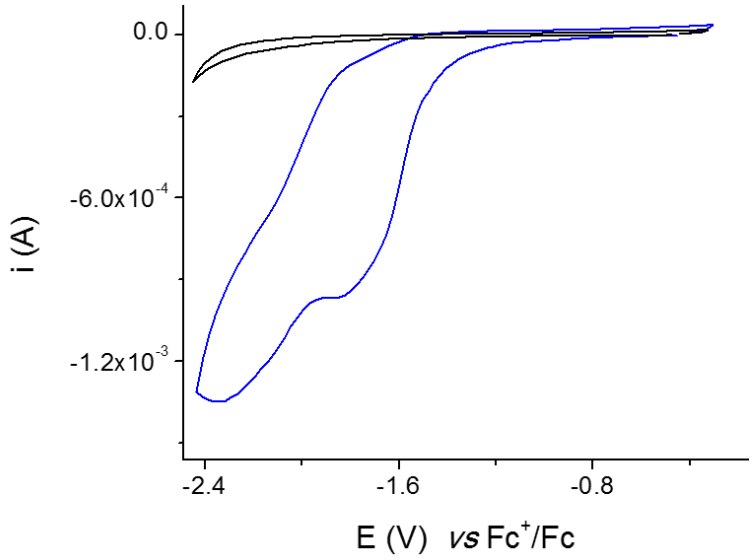

Figure ES10. CV of complex **C3** (1 mM) (blue) and CV of 20 mM of TFA (black) in the absence of the complex. The CVs were recorded in CH_3CN at 30 V s^{-1} and 0.1 M $TBAPF_6$ in acetonitrile, with glassy carbon working electrode.

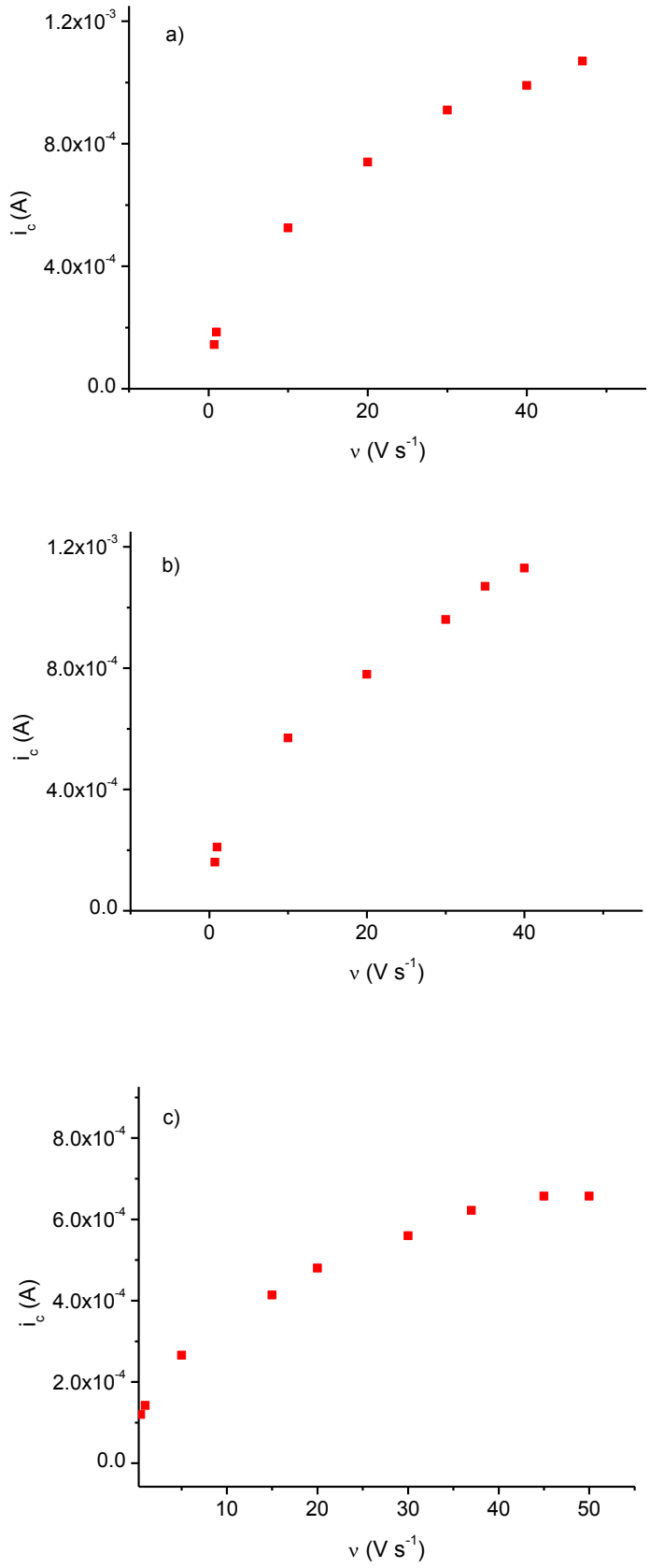

Figure ES11. Catalytic current versus the scan rate for the CVs of 1 mM **C2** and 20 mM TFA (a), 1 mM **C3** and 20 mM TFA (b) and 1 mM **C4** and 15 mM TFA (c).

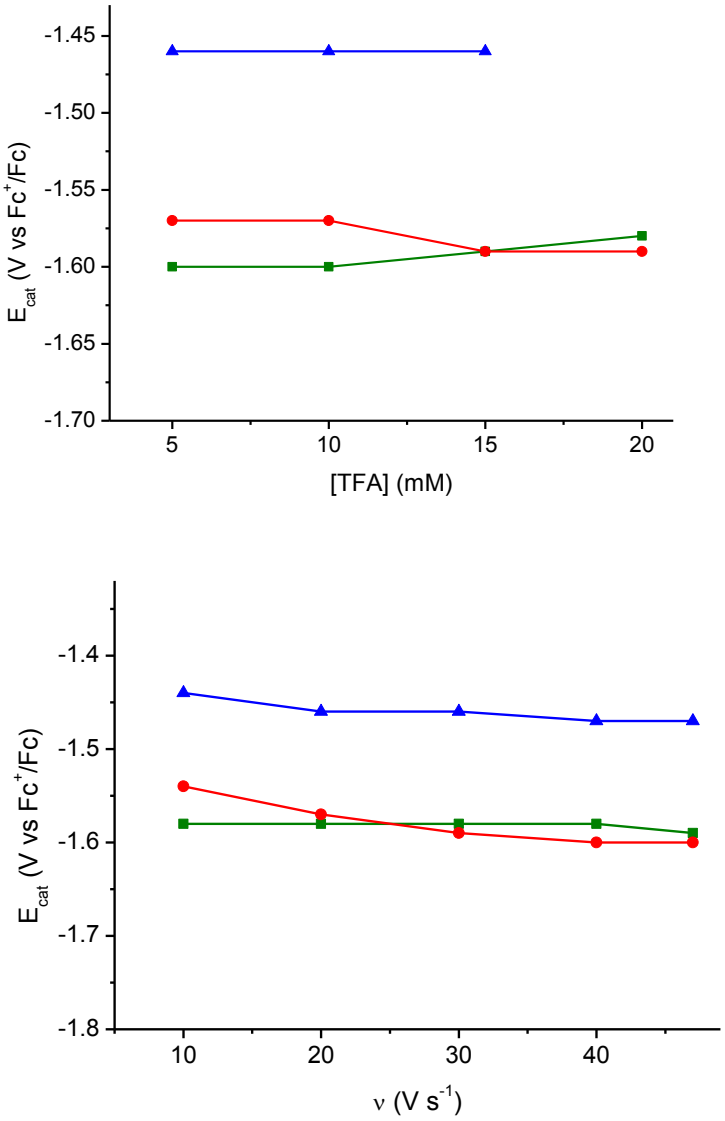

Figure ES12. Top: E_{cat} versus concentration of TFA. Bottom: E_{cat} versus scan rate. **C2** red, **C3** green, **C4** blue.

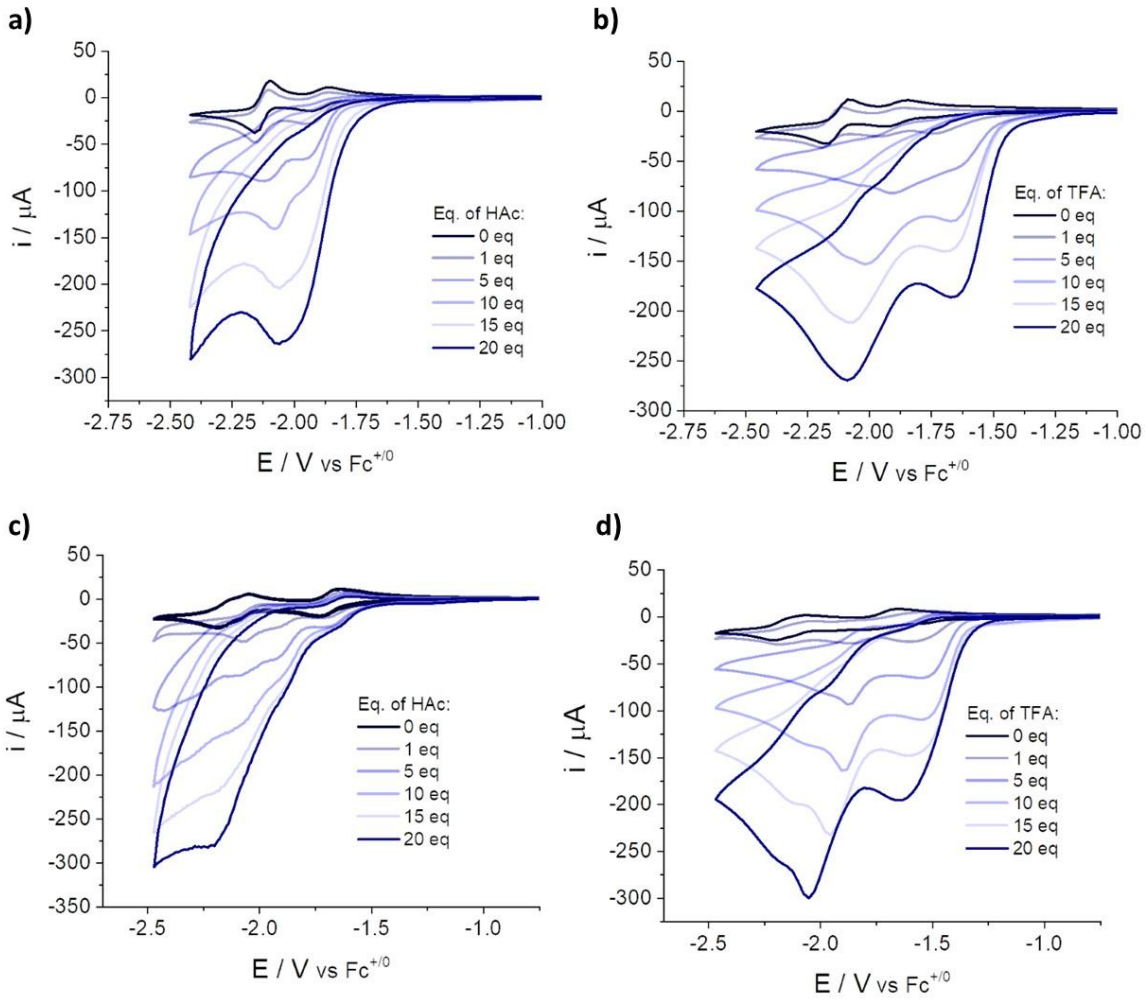

Figure ES13. a) CV of **C2** (1 mM) in the presence of acetic acid (HAc, E_{cat} = -1.88 V) and b) of trifluoroacetic acid (TFA). c) CV of **C4** (1 mM) in the presence of acetic acid (HAc, E_{cat} = -1.62 V) and d) of trifluoroacetic acid (TFA). CVs were recorded in CH_3CN at 100 mV s^{-1} and 0.1 M $TBAPF_6$ in acetonitrile, with glassy carbon working electrode.

S 6. Photochemical H_2 evolution

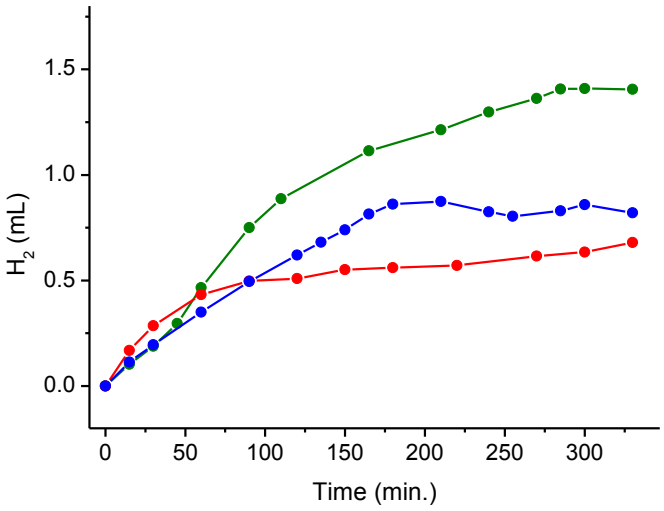

Figure ES14. H_2 evolution in mL over time for 5 μM **C1** (blue) **C3** (green), **C4** (red), 1.0 M acetate buffer at pH 4.0 with 0.1 M of ascorbic acid and 0.5 mM $[Ru(bpy)_3]Cl_2$ at 20°C, LED light at 475 nm in the presence of 1 mL Hg.

S 7. Crystallographic data

Table ES2. Crystallographic data.

	C2	**C3''**	**C4**	**C4'**
Empirical formula	$C_{29}H_{23}BCoF_4N_6O_2$	$C_{29}H_{26}CoF_{12}N_6OP_2$	$C_{29}H_{28}B_2CoF_8N_6O_2$	$C_{28}H_{24}CoN_6O_5S$
Formula weight	633.27	823.43	725.12	615.52
Crystal system	monoclinic	orthorhombic	monoclinic	monoclinic
Space group	$P2_1/c$	Pnma	$P2_1/n$	$P2_1/c$
Unit cell dimensions (Å)	*a* = 10.55106(10)	*a* = 11.3970(3)	*a* = 13.4225(3)	*a* = 10.3063(3)
	b = 18.59568(18)	b = 39.0957(13)	b = 12.9039(3)	b = 14.6574(5)
	c = 13.49144(12)	c = 14.0077(4)	c = 21.6590(5)	c = 23.7054(8)
	α = 90°	α = 90°	α = 90°	α = 90°
	β = 94.1708(8)°	β = 90°	β = 93.254(2)°	β = 92.438(3)°
	γ = 90°	γ = 90°	γ = 90°	γ = 90°
Volume ($Å^3$)	2640.07(4)	6241.5(3)	3745.34(15)	3577.8(2)
Density calculated (g/cm^3)	1.593	1.753	1.286	1.143

Table ES3. Selected bond lengths (Å) in crystal structures.

C2	**C3''**	**C4**	**C4'**

Co-O1	2.1488(11)	Co-O1	2.2928(15)	Co-N1	2.236(2)	Co-O2	2.0102(14)
Co-N1	2.4101(13)	Co-N1	2.3080(17)	Co-N2	2.077(2)	Co-N1	2.2378(19)
Co-N2	2.1341(12)	Co-N2	2.1191(18)	Co-N3	2.274(2)	Co-N2	2.1167(18)
Co-N3	2.2987(13)	Co-N3	2.2337(17)	Co-N4	2.072(2)	Co-N3	2.3393(18)
Co-N4	2.1644(13)	Co-N4	2.1133(16)	Co-N5	2.238(2)	Co-N4	2.0667(17)
Co-N5	2.2623(12)	Co-N5	2.2631(16)	Co-N6	2.097(2)	Co-N5	2.1761(17)
Co-N6	2.1191(13)	Co-N6	2.1219(17)				

Table ES4. Selected angles (degrees) in crystal structures.

C2		**C3''**		**C4**		**C4'**	
N2—Co—N5	158.73(5)	N2—Co—N5	92.66(6)	N1—Co—N6	131.13(9)	N1—Co—N3	140.74(7)
N1—Co—N5	126.97(5)	N6—Co—N2	116.83(7)	N1—Co—N5	83.02(8)	N1—Co—N5	85.76(7)
N6—Co—N5	92.33(5)	N1—Co—N5	134.20(6)	N1—Co—N4	104.96(9)	N1—Co—N4	98.38(7)
N5—Co—N3	85.11(5)	N6—Co—N1	72.16(7)	N1—Co—N3	143.09(9)	O2—Co—N1	101.20(7)
N4—Co—N5	72.23(5)	N2—Co—N3	72.76(6)	N1—Co—N2	74.90(8)	N1—Co—N2	74.90(7)
N4—Co—N1	69.82(5)	N4—Co—N2	109.63(6)	N5—Co—N6	89.48(9)	N2—Co—N5	160.47(7)
N4—Co—N3	93.40(5)	O1—Co—N3	84.97(6)	N4—Co—N6	119.01(10)	N2—Co—N4	110.74(7)
N6—Co—N4	111.93(5)	O1—Co—N4	88.41(6)	N6—Co—N3	73.94(9)	N2—Co—N3	72.78(7)
N2—Co—N4	108.53(5)	N1—Co—N3	124.58(6)	N2—Co—N6	98.87(9)	O2—Co—N2	91.30(7)
N6—Co—N3	152.48(5)	N1—Co—N4	72.02(6)	N5—Co—N4	73.67(9)	N3—Co—N5	126.04(7)
N2—Co—N3	73.62(5)	N6—Co—N3	88.71(6)	N5—Co—N3	129.07(9)	N3—Co—N4	73.33(7)
N1—Co—N3	132.17(5)	N6—Co—N4	105.47(6)	N2—Co—N5	156.48(9)	O2—Co—N3	101.23(7)
N6—Co—N2	106.41(5)	N5—Co—N6	147.62(7)	N4—Co—N3	73.57(9)	N4—Co—N5	74.29(7)
N6—Co—N1	69.79(5)	N5—Co—N4	74.05(6)	N2—Co—N4	119.59(9)	O2—Co—N5	89.78(6)
N2—Co—N1	70.53(5)	O1—Co—N6	71.45(6)	N2—Co—N3	74.46(9)	O2—Co—N4	153.71(7)
O1—Co—N2	88.39(5)	O1—Co—N5	76.17(6)				
O1—Co—N1	77.472(0)	O1—Co—N1	131.73(6)				
O1—Co—N5	86.826(0)	O1—Co—N2	155.57(6)				
O1—Co—N4	157.906(0)	N4—Co—N3	161.56(6)				
O1—Co—N3	130.89()	N5—Co—N6	147.62(7)				
O1—Co—N6	75.024(0)	N1—Co—N2	74.087(1)				

S 8. Spectroscopic data

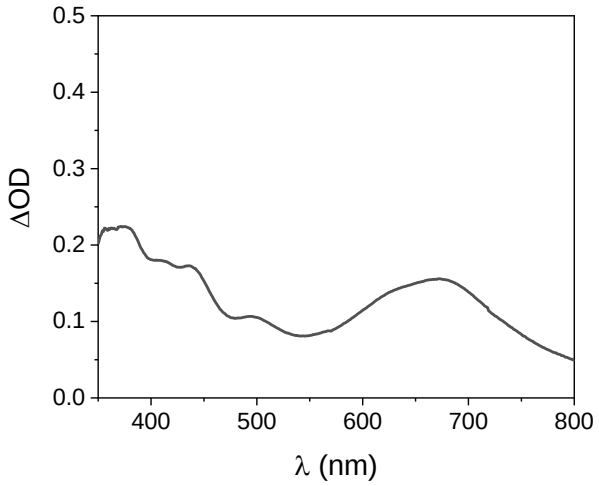

Figure ES15. Differential UV-Vis absorption spectrum obtained by spectroelectrochemistry of 1 mM complex **C1** in acetonitrile (optical pathlength = 0.5 mm) upon application of -1.7 V vs Fc^{+}/Fc.

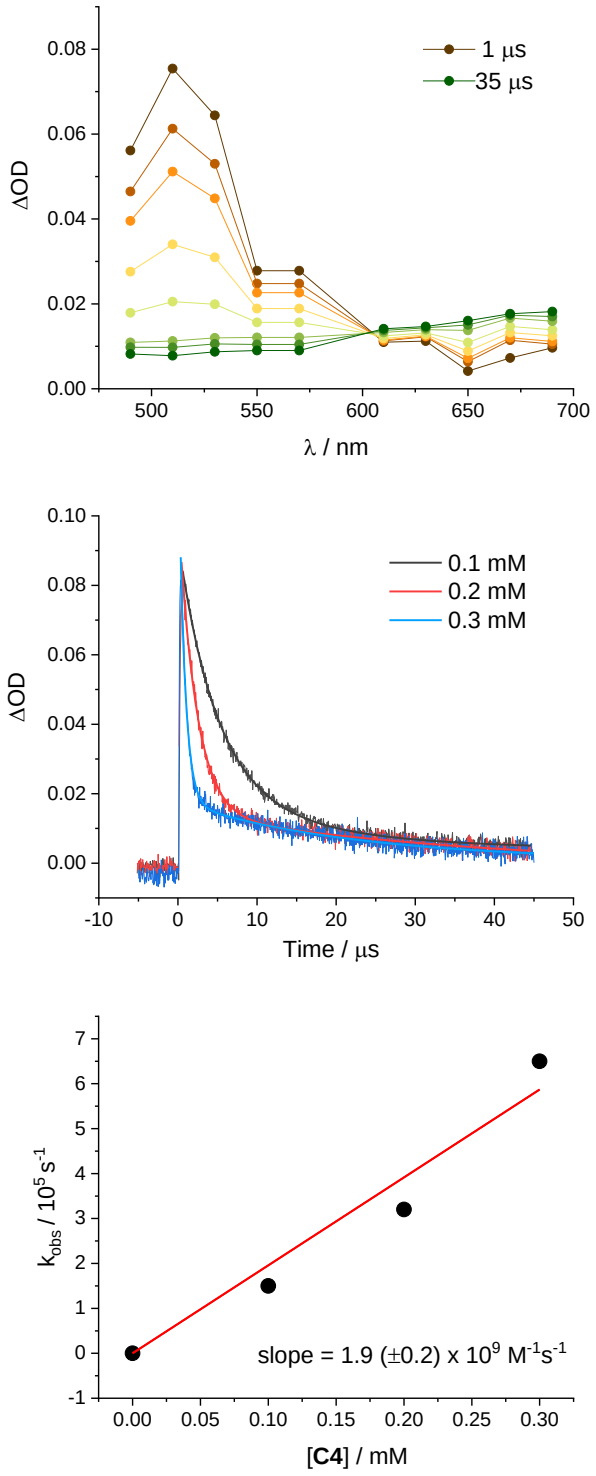

Figure ES16. Transient absorption spectra between 1-35 μs obtained by laser flash photolysis (excitation at 532 nm) of a solution containing 70 μM $[Ru(bpy)_3]^{2+}$, 0.1 M ascorbic acid, and 0.1 mM **C4** in 1 M acetate buffer (top); kinetic traces at 510 nm at 0.1-0.3 mM **C4** (middle), the fitting was performed using a biexponential function in which the first component is associated to the reaction in eq. 3 of the main article, the second component to the charge recombination between Co(I) and the ascorbate radical; plot of the observed rate (extracted from the first time component of the fitting of the kinetic traces) vs. catalyst concentration for the estimation of the bimolecular rate constant for electron transfer from photogenerated $[Ru(bpy)_3]^{+}$ to **C4** (bottom).

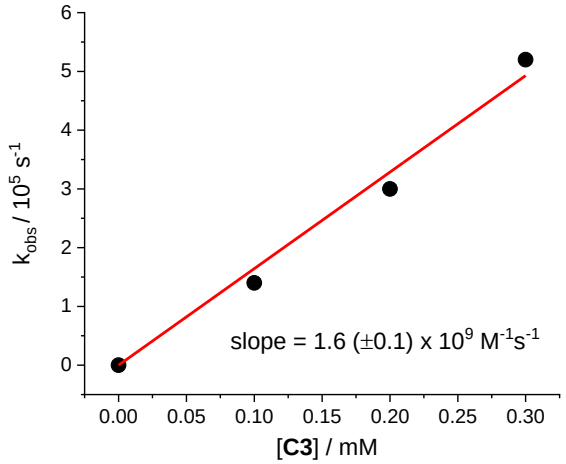

Figure ES17. Plot of the observed rate (extracted from the first time component of the fitting of the kinetic traces in Figure 8b of the main article) vs. catalyst concentration for the estimation of the bimolecular rate constant for electron transfer from photogenerated $[Ru(bpy)_3]^+$ to **C3**.

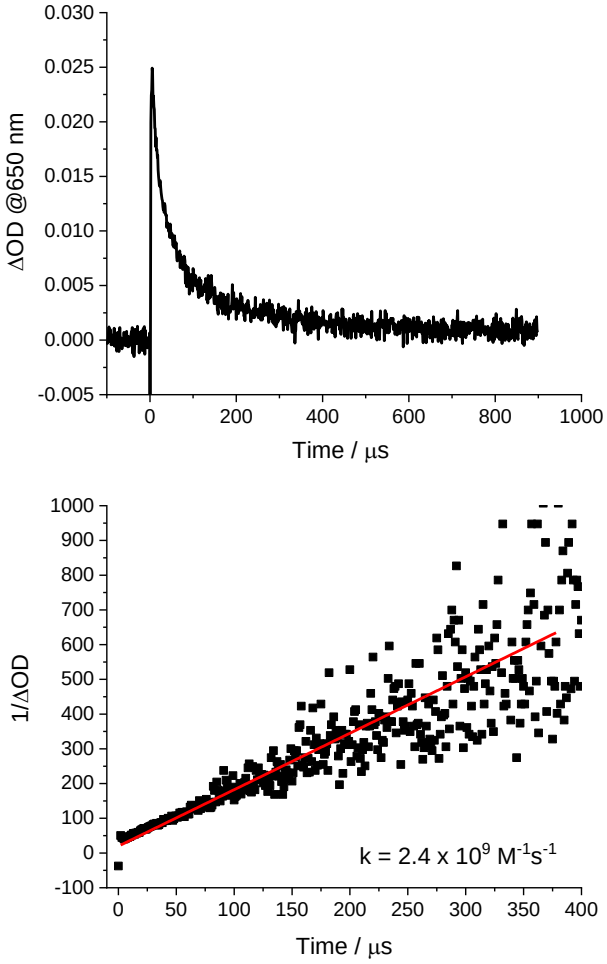

Figure ES18. Kinetic trace at 650 nm accounting for the charge recombination between reduced **C3** and the ascorbate radical (top); second-order kinetic treatment for the estimation of the bimolecular rate constant (bottom), an optical pathlength l = 0.74 and a $\Delta\varepsilon$ = 2000 $M^{-1}cm^{-1}$ were considered.

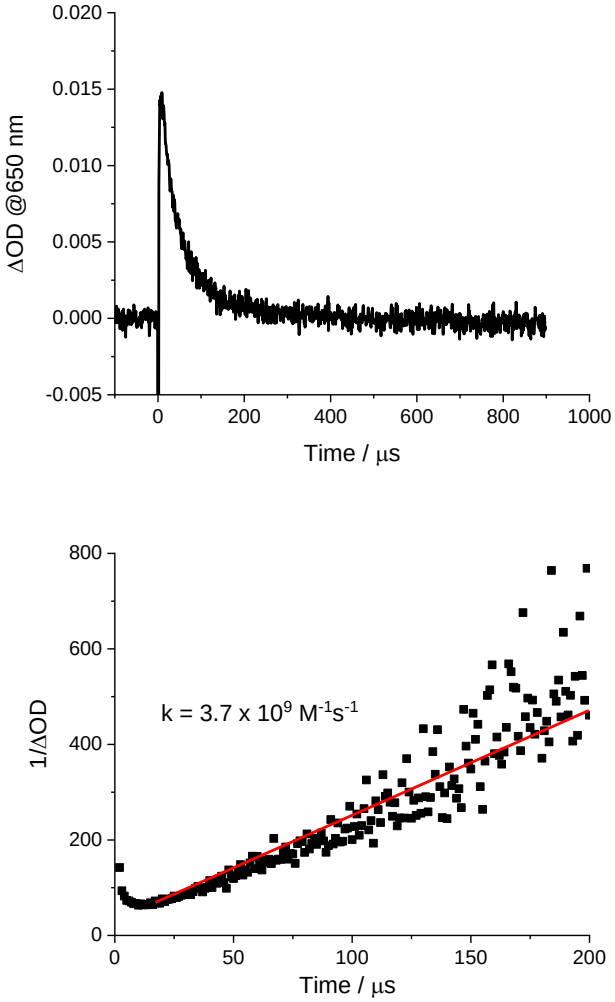

Figure ES19. Kinetic trace at 650 nm accounting for the charge recombination between reduced **C4** and the ascorbate radical (top); second-order kinetic treatment for the estimation of the bimolecular rate constant (bottom), an optical pathlength l = 0.74 and a $\Delta\varepsilon$ = 2000 $M^{-1}cm^{-1}$ were considered.

S9. Computational data

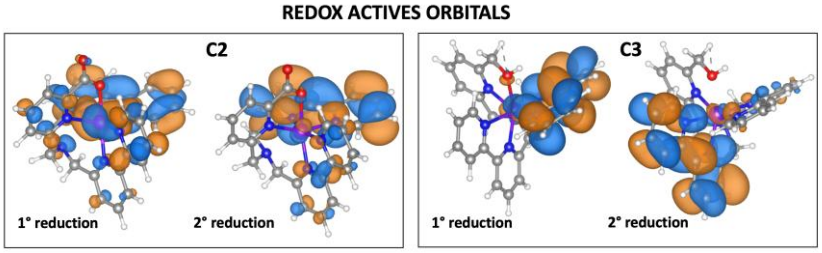

Figure ES20. Isodensity surface plots of the Redox active orbitals (PBE0/6-311G**/Acetonitrile) for the first and second reduction of **C2** and **C3**.

Table ES5. Calculated energy differences (ΔE, eV) in acetonitrile between the high (HS) and low (LS) spin states of **C2** and **C3** complexes. For the sake of consistency, the experimental geometry has been used for both PBE0 and MP2 single point calculations.

Molecule	**ΔE_{HS-LS} (eV)**	
	PBE0/6-311G*	**MP2/6-311G***
C2	-1.74	-6.5
C3	-1.85	-2.31

Table ES6. Calculated free energy differences in acetonitrile for the possible reaction steps involved in the proposed mechanisms. All the values are in eV.

Reaction Steps	ΔG vs vacuum	ΔG vs NHE	Sum of ΔG vs NHE
C2 – ECEC (initially protonated)			
Co(II)-OfH + e^- → Co(I)-OfH	-3.209	1.231	1.231
Co(I)-OfH + H^+ → Co(I)-PYH-OfH	0.333	0.333	1.564
Co(I)-PYH-OfH + e^- → Co(I)-$PY^{(-)}$H-OfH	-3.382	1.058	2.261
Co(I)-OfH + H^+ → Co(I)-BPY2H-OfH	0.211	0.211	1.441
Co(I)-BPY2H-OfH + e^- → Co(I)-$BPY2^{(-)}$H-OfH	-3.537	0.903	2.344
Co(I)-OfH + H^+ → Co(I)-BPY1H-OfH	0.118	0.118	1.349
Co(I)-BPY1H-OfH + e^- → Co(I)-$BPY1^{(-)}$H-OfH	-3.362	1.078	2.427
C2 – ECEC (non-initially protonated)			
Co(II) + e^- → Co(I)	-2.733	1.706	1.706
Co(I) + H^+ → Co(I)-OfH	-0.415	-0.415	1.291
Co(I)-OfH + e^- → Co(I)-$Of^{(-)}$H	-2.332	2.108	3.399
Co(I) + H^+ → Co(I)-OcH	-0.272	-0.272	1.435
Co(I)-OcH + e^- → Co(I)-$Oc^{(-)}$H	-2.580	1.860	3.295
C2 – CEEC (non-initially protonated)			
Co(II) + H^+ → Co(II)-OfH	-1.684	-1.684	-1.684
Co(II)-OfH + e^- → Co(I)-OfH	-3.209	1.231	-0.453
Co(I)-OfH + e^- → Co(I)-$Of^{(-)}$H	-2.332	2.108	1.655
Co(II) + H^+ → Co(II)-OcH	0.114	0.114	0.114
Co(II)-OcH + e^- → Co(I)-OcH	-3.119	1.321	1.435
Co(I)-OcH + e^- → Co(I)-$Oc^{(-)}$H	-2.580	1.860	3.295
C3 - ECEC			
Co(II) + e^- → Co(I)	-2.956	1.484	1.484
Co(I) + H^+ → Co(I)-BPY1H	-0.095	-0.095	1.389
Co(I)-BPY1H + e^- → Co(I)-$BPY1^{(-)}$H	-3.520	0.920	2.309

ΔGs vs vacuum have been calculated according to the procedure proposed by Muckerman and Fujita.[15]

ΔGs vs NHE have been calculated from the values vs vacuum by using the conversion factor -4.44 V.

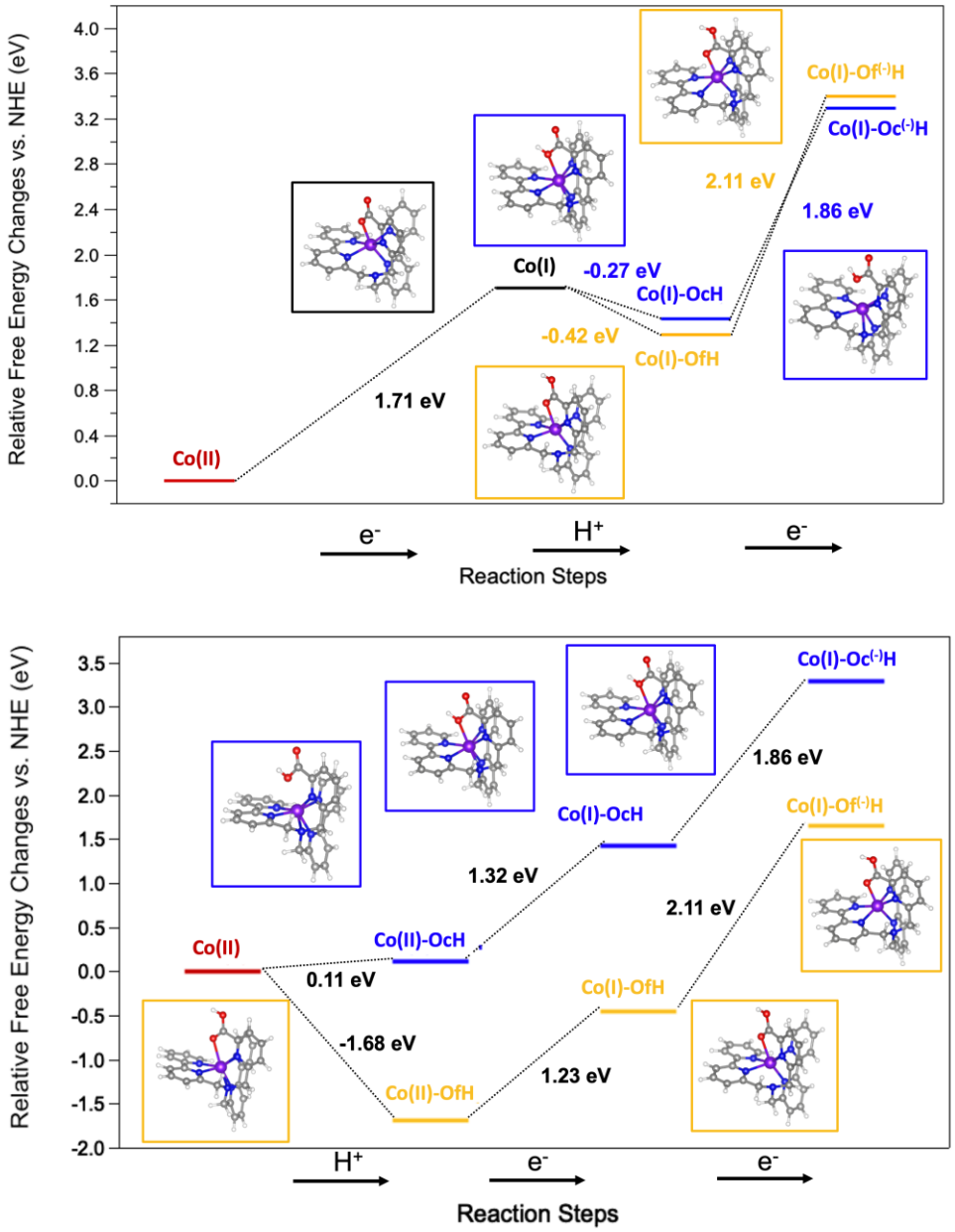

Figure ES21. Calculated free energies profiles (in eV) for the possible **C2** reaction steps involved in the ECEC mechanism (top) or in the CEEC mechanism (bottom), starting from a non-initially protonated complex. Values of the relative free energy changes *vs* NHE are given in Table ES6.

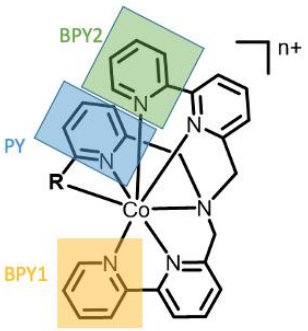

Figure ES22. Scheme of the nomenclature used to design the protonated N sites on the ligands.

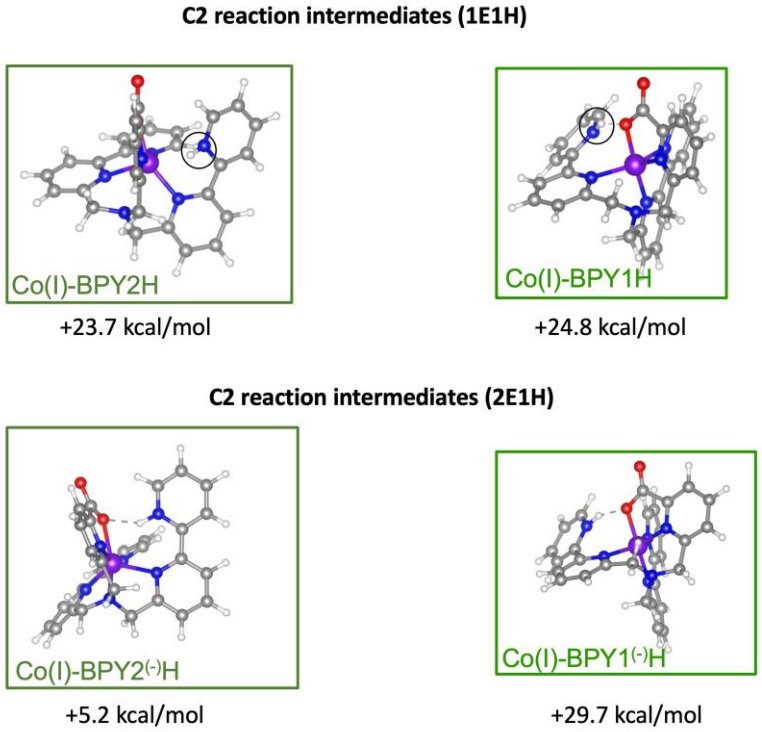

Figure ES23. Optimized structures of other stable protonated intermediates calculated for **C2**. The relative stability (kcal/mol) with respect to **Co(I)-OfH** (1E1H) and **Co(I)-Of$^{(-)}$H** (2E1H) is also given.

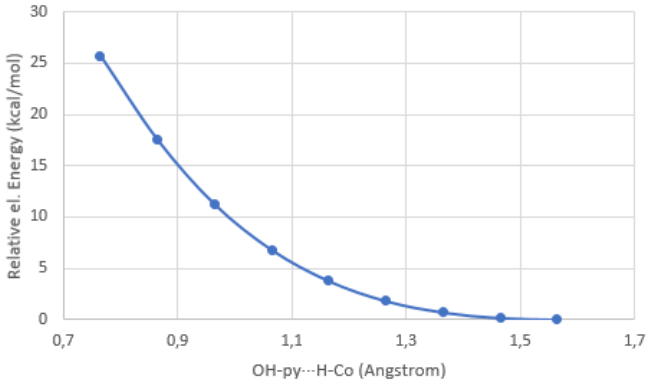

Figure ES24. Unproductive **C3** path toward H_2 production from **Co(II)H-BPY1H**, as a function of the Co-H···HO-CH_2-py distance coordinate.

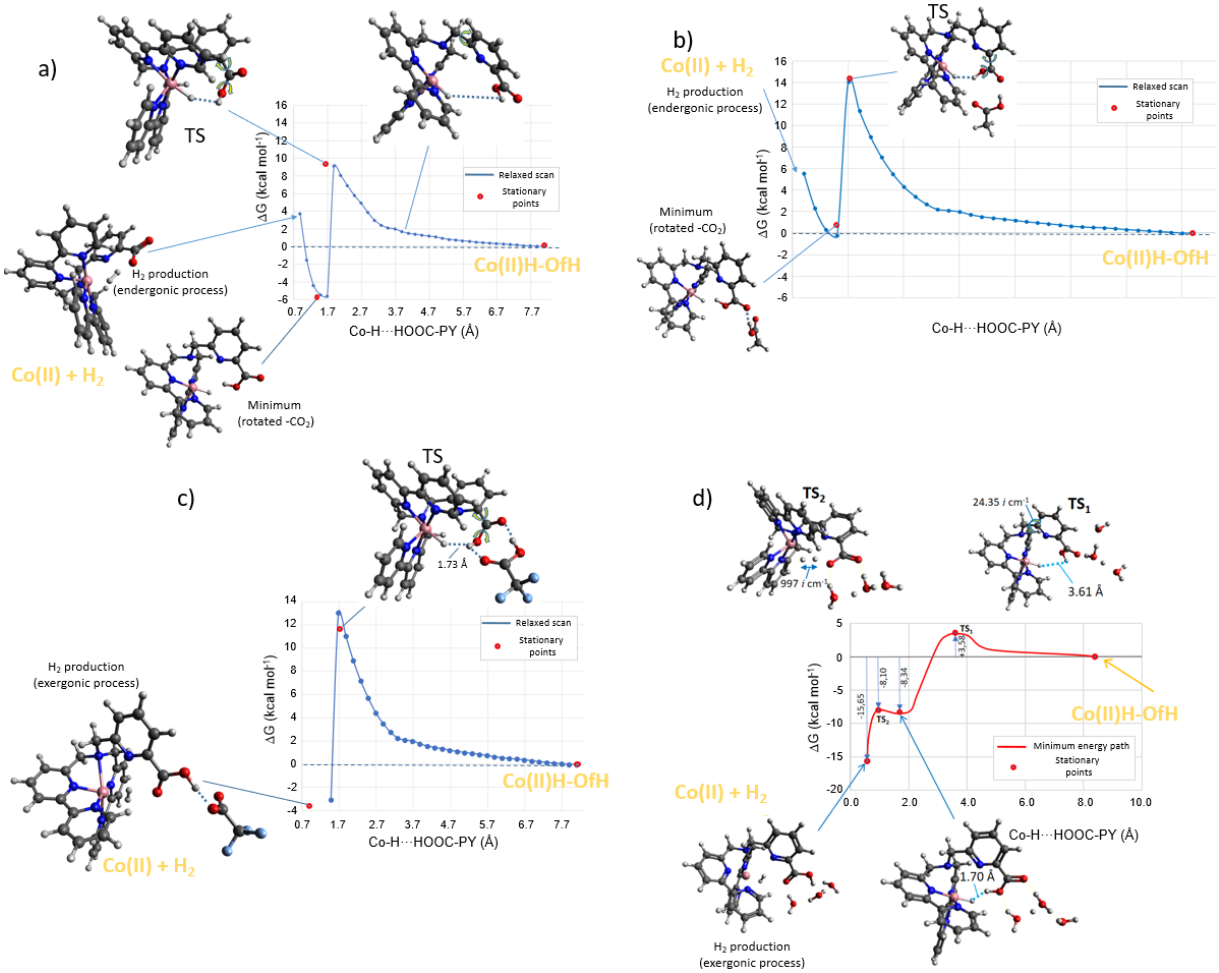

Figure ES25. **C2** paths toward H_2 production (from right to left), starting from **Co(II)H-OfH**, in terms of relative free energy changes (ΔG) as a function the Co-H···HOOC-PY distance coordinate, depending on the acidic environment: a) no acidic surrounding; b) with a CH_3COOH molecule (weak acid); c) with a CF_3COOH (TFA) molecule (strong acid).; d) with a $(H_2O)2(H_3O^+)$ cluster (strong acidic medium).

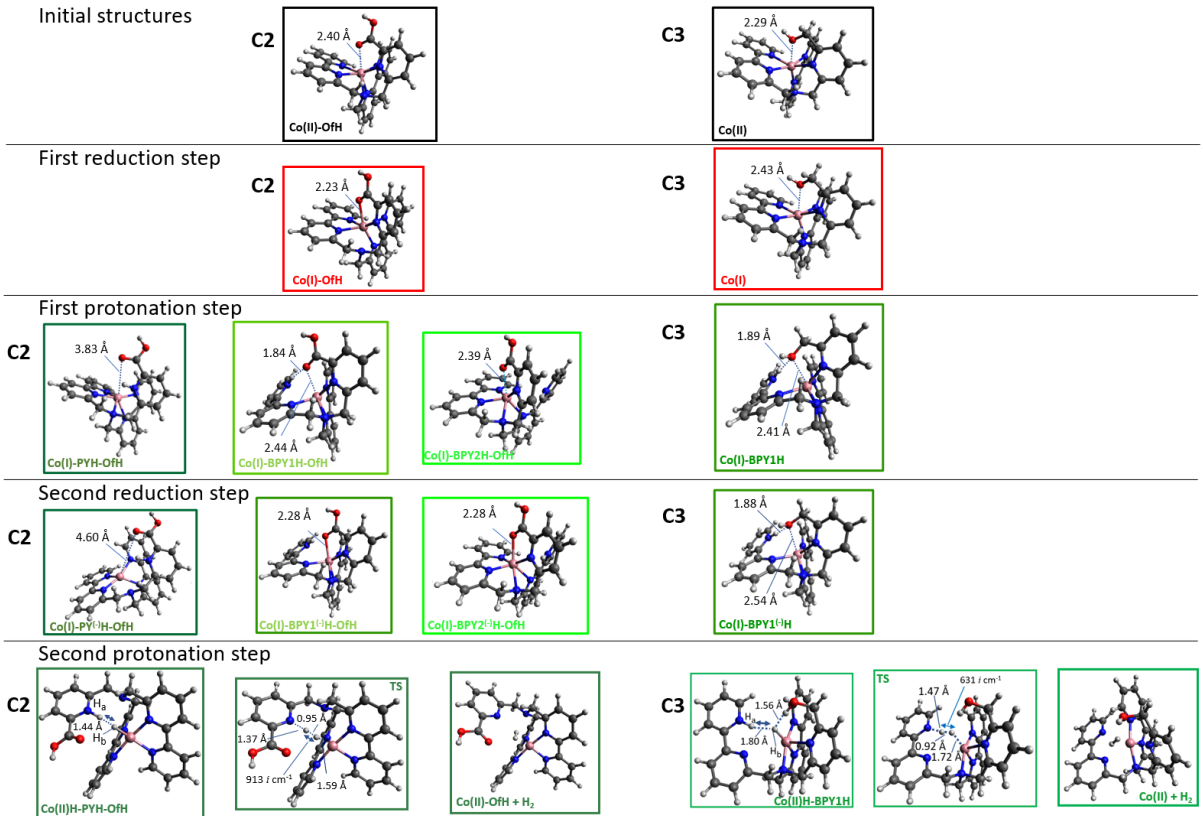

Figure ES26. Structures and main geometrical parameters corresponding to the species of Figs. 9 and 10 of the main text.

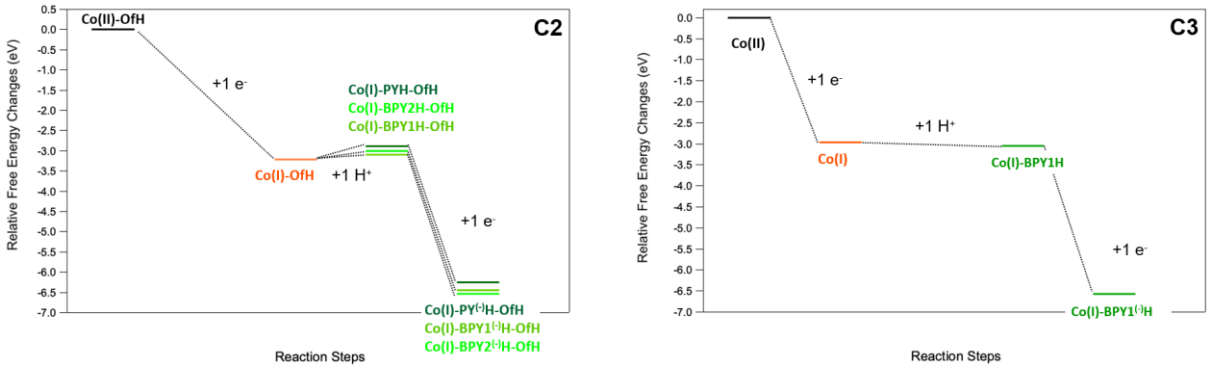

Figure ES27. Calculated free energy profiles (ΔG vs vacuum) for **C2** (left) and **C3** (right), corresponding to first reduction, first protonation, and second reduction steps. Numerical values are available in Table ES6.

S 10. References

1. G. Sheldrick, *Acta Cryst.*, 2015, **C71**, 3-8.
2. O. V. Dolomanov, L. J. Bourhis, R. J. Gildea, J. A. K. Howard and H. Puschmann, *J. Appl. Cryst.*, 2009, **42**, 339-341.
3. G. Sheldrick, *Acta Cryst.*, 2015, **A71**, 3-8.
4. M. D. Best and E. V. Anslyn, *Chem. Eur. J.*, 2003, **9**, 51-57.
5. S. Kulyk, W. G. Dougherty, W. S. Kassel, M. J. Zdilla and S. M. Sieburth, *Org. Lett.*, 2011, **13**, 2180-2183.
6. X. S. Zeng, D. Coquiere, A. Alenda, E. Garrier, T. Prange, Y. Li, O. Reinaud and I. Jabin, *Chem. Eur. J.*, 2006, **12**, 6393-6402.
7. F. Lucarini, M. Pastore, S. Vasylevskyi, M. Varisco, E. Solari, A. Crochet, K. M. Fromm, F. Zobi and A. Ruggi, *Chem. Eur. J.*, 2017, **23**, 6768-6771.
8. K. De Buysser, G. G. Herman, E. Bruneel, S. Hoste and I. Van Driessche, *Chem. Phys.*, 2005, **315**, 286-292.
9. K. C. de Berg and K. J. Chapman, *J. Chem. Educ.*, 2001, **78**, 670-673.
10. M. Vennampalli, G. Liang, L. Katta, C. E. Webster and X. Zhao, *Inorg. Chem.*, 2014, **53**, 10094-10100.
11. F. Lucarini, J. Fize, A. Morozan, M. Marazzi, M. Natali, M. Pastore, V. Artero, A. Ruggi, *Sustain. Energy Fuels,* 2020, **4**, 589-599.
12. C. Costentin, J.-M. Savéant, *ChemElectroChem,* 2014, **1**, 1226-1236.
13. C. Costentin, S. Drouet, M. Robert, J.-M. Savéant, *J. Am. Chem. Soc.,* 2012**, 134**, 11235-11242.
14. V. Artero, J.-M. Savéant, *Energy Environ. Sci.,* 2014, **7**, 3808-3814.
15. J. T. Muckerman, E. Fujita, *Chem Comm.* 2011, **47**, 12456-12458.